Comparative oncogenomics identifies tyrosine kinase FES as a tumor suppressor in melanoma

Michael Olvedy,[1,2] Julie C. Tisserand,[3] Flavie Luciani,[1,2] Bram Boeckx,[4,5] Jasper Wouters,[6,7] Sophie Lopez,[3] Florian Rambow,[1,2] Sara Aibar,[6,7] Bernard Thienpont,[4,5] Jasmine Barra,[1,2] Corinna Köhler,[1,2] Enrico Radaelli,[8] Sophie Tartare-Deckert,[9] Stein Aerts,[6,7] Patrice Dubreuil,[3] Joost J. van den Oord,[10] Diether Lambrechts,[4,5] Paulo De Sepulveda,[3] and Jean-Christophe Marine[1,2]

[1]Laboratory for Molecular Cancer Biology, Center for Cancer Biology, Vlaams Instituut voor Biotechnologie (VIB), Leuven, Belgium. [2]Laboratory for Molecular Cancer Biology, Department of Oncology, KU Leuven, Leuven, Belgium. [3]INSERM, Aix Marseille University, CNRS, Institut Paoli-Calmettes, CRCM, Equipe Labellisée Ligue Contre le Cancer, Marseille, France. [4]Laboratory for Translational Genetics, Center for Cancer Biology, VIB, Leuven, Belgium. [5]Laboratory for Translational Genetics, [6]Laboratory of Computational Biology, Department of Human Genetics, KU Leuven, Leuven, Belgium. [7]Laboratory of Computational Biology, [8]Mouse Histopathology Core Facility, VIB Center for Brain & Disease Research, Leuven, Belgium. [9]Centre Méditerranéen de Médecine Moléculaire (C3M), INSERM, U1065, Université Côte d'Azur, Nice, France. [10]Laboratory of Translational Cell and Tissue Research, Department of Pathology, KU Leuven and UZ Leuven, Leuven, Belgium.

Identification and functional validation of oncogenic drivers are essential steps toward advancing cancer precision medicine. Here, we have presented a comprehensive analysis of the somatic genomic landscape of the widely used $BRAF^{V600E}$- and $NRAS^{Q61K}$-driven mouse models of melanoma. By integrating the data with publically available genomic, epigenomic, and transcriptomic information from human clinical samples, we confirmed the importance of several genes and pathways previously implicated in human melanoma, including the tumor-suppressor genes phosphatase and tensin homolog (*PTEN*), cyclin dependent kinase inhibitor 2A (*CDKN2A*), *LKB1*, and others. Importantly, this approach also identified additional putative melanoma drivers with prognostic and therapeutic relevance. Surprisingly, one of these genes encodes the tyrosine kinase FES. Whereas FES is highly expressed in normal human melanocytes, FES expression is strongly decreased in over 30% of human melanomas. This downregulation correlates with poor overall survival. Correspondingly, engineered deletion of *Fes* accelerated tumor progression in a $BRAF^{V600E}$-driven mouse model of melanoma. Together, these data implicate FES as a driver of melanoma progression and demonstrate the potential of cross-species oncogenomic approaches combined with mouse modeling to uncover impactful mutations and oncogenic driver alleles with clinical importance in the treatment of human cancer.

Introduction

Genome-wide scans and resequencing efforts have recently revealed hundreds of recurrent copy-number alterations (CNAs) and point mutations across diverse human cancers. However, genomic instability and heterogeneity of human tumors impedes a straightforward cataloguing of cancer-causing genes and of possible therapeutic targets. Strategies enabling the distinction of causal genetic alterations (drivers) from bystander genomic noise (passengers) are needed to facilitate the discovery of genes that drive oncogenesis. Although several approaches have recently been described, the statistical power of these approaches depends on very large sample numbers (1). Another major limitation of human cancer-genome characterization studies is the lack of rigorous in vivo functional validation. Studies that include functional data invariably rely upon transfection studies in cultured cells, which lack many hallmarks of naturally arising tumors (2). There is therefore the pressing need to combine comparative oncogenomic approaches with in vivo cancer models to identify and validate new bona fide cancer genes/pathways that drive cancer progression and/or metastasis.

Malignant melanoma is one of the most aggressive and treatment-resistant human cancers. Improvement of clinical outcomes for this disease remains a major challenge. Despite the recent developments in melanoma therapies, most of the patients with metastatic melanoma still succumb to their disease (3). The molecular genetics of melanoma, and in particular how specific genomic and nongenomic (epigenetic) alterations interact to produce its aggressive/metastatic characteristics, remain poorly understood. This lack of knowledge has been a major barrier to rational development of effective therapeutics and prognostic diagnostics for melanoma patients. One confounding factor of discriminating drivers in human melanoma is the particularly high background mutation burden due to UV mutagenesis (4).

Substantial progress in our understanding of the etiologies and genetic underpinnings of melanoma has nevertheless been made and has led to promising results in trials of targeted therapies for this disease. A key advance was the discovery of the recurrent somatic mutations in the gene encoding the BRAF serine-threonine kinase, the $BRAF^{V600E}$ mutation being the most common, in about 50% of patients (5). Large single-center studies, meta-analyses, and whole-exome sequencing (WES) efforts have

Authorship note: M. Olvedy, J.C. Tisserand, and F. Luciani are co–first authors. D. Lambrechts, P. De Sepulveda, and J.C. Marine are co–senior authors.
Conflict of interest: The authors have declared that no conflict of interest exists.
Submitted: October 21, 2016; **Accepted:** March 2, 2017.
Reference information: *J Clin Invest*. https://doi.org/10.1172/JCI91291.

subsequently confirmed that $BRAF^{V600E}$ mutations are among the most common activating genetic events detected in cutaneous melanomas (4, 6–8). Accordingly, mice engineered to express $BRAF^{V600E}$ in melanocytes develop melanoma at a median latency of 12.6 months (9). This mutation overactivates the MAPK/ERK signaling pathway, leading to melanocytic hyperproliferation (10). Importantly, $BRAF^{V600E}$-mutant melanomas are addicted to this oncogenic driver mutation and targeted therapies against the $BRAF^{V600E}$-activated oncogene have demonstrated very effective antitumor responses in patients (11, 12). Activation of the MAPK signaling pathway in about 20% of cutaneous melanoma is a consequence of NRAS mutations (6), and melanocyte-specific expression of $NRAS^{Q61K}$ drives melanoma formation in mice (13).

Both $BRAF^{V600E}$- and $NRAS^{Q61K}$-driven mouse melanoma lesions recapitulate many histopathological features that are seen in subsets of human melanomas (9, 13–15). The long latency in these models (>10 months) indicates that additional genomic alterations are required for tumor progression. Loss-of-function mutations in phosphatase and tensin homolog (PTEN), cyclin dependent kinase inhibitor 2A (CDKN2A), or cyclin-dependent kinase inhibitor 2A (INK4A) and transformation related protein 53 (TRP53), events that are frequently observed in human melanoma (16), have been shown to increase the penetrance and reduce the latency of these $BRAF^{V600E}$- and/or $NRAS^{Q61K}$-driven mouse melanoma lesions (13, 14, 17–20). Importantly, since these melanoma lesions develop in the absence of UV exposure, the background mutation frequency is likely to be dramatically reduced. We therefore hypothesized that these models are well suited for a comparative cancer genome study aimed at identifying genetic events that drive melanoma initiation and progression in cooperation with oncogenic BRAF and NRAS and, importantly, validating their relevance in the appropriate in vivo context.

Results

Low mutation burden in murine melanoma. In an effort to identify novel melanoma drivers, $BRAF^{V600E}$- and $NRAS^{Q61K}$-driven spontaneous cutaneous melanoma mouse lesions were subjected to WES at an average coverage depth of ×60 (Supplemental Table 1; supplemental material available online with this article; https://doi.org/10.1172/JCI91291DS1). $BRAF^{V600E}$-driven lesions lacking $p16^{INK4A}$ (thereafter referred to as INK4A) in the melanocyte lineage (*Tyr-Cre*$^{ERT2/°}$ *Braf*$^{LSL\text{-}V600E/+}$ *Ink4a*$^{-/-}$ mice) and $NRAS^{Q61K}$–melanoma lacking both *Trp53* alleles (*Trp53*-null) in the melanocyte lineage (*Tyr-Cre Tyr-Nras*$^{Q61K/°}$ *Trp53*$^{fl/fl}$ mice) were also analyzed (21, 22). Note that although the loss of these tumor suppressors accelerated melanomagenesis, frank cutaneous melanoma lesions only appeared on average after 57 weeks in the absence of *Ink4a* and after 30 weeks on the *Trp53*-null background. In total, 8 $BRAF^{V600E}$-driven (2 of which originated from the same mouse) and 4 $NRAS^{Q61K}$-driven melanoma lesions were sequenced (Supplemental Figure 1A). We also sequenced matching germline DNA from each intercross (4 *Tyr-Cre*$^{ERT2/°}$ *Braf*$^{LSL\text{-}V600E/+}$ *Ink4a*$^{-/-}$, 2 *Tyr-Nras*$^{Q61K/°}$ and 2 *Tyr-Cre Tyr-Nras*$^{Q61K/°}$ *Trp53*$^{fl/fl}$) at an average coverage depth of ×60. We identified all somatic variants in these 12 melanoma lesions using an established pipeline that had been previously used to reliably identify a large number of carcinogen-induced somatic mutations in mouse squamous cell carcinomas (23).

Strikingly, somatic variants were rare in all lesions, with an average of 1.33 missense mutations per lesion (Supplemental Figure 1A). In total, 16 mutations were identified and independently validated using an orthogonal genotyping method. Notably, loss of *Trp53* did not significantly increase the number of missense mutations (Supplemental Figure 1A and Supplemental Table 2). Likewise, we identified and independently validated only 1 single indel across all 12 lesions. This indel caused a frameshift deletion in *Fbxw22* and is predicted to cause a loss-of-function phenotype (Supplemental Figure 1A). The number of missense mutations in each lesion was significantly lower than in sun-exposed human melanoma (8). Similarly to non–sun-exposed human melanoma (8), we failed to identify a specific mutational signature or mutational bias (Supplemental Figure 1B), due to low mutation burden.

Consistent with the low mutation burden, we identified only 1 recurrent missense mutation in *A230050P20Rik*. However, this mutation was found in 2 different tumors isolated from the same mouse, indicating that these lesions are likely to be clonally related as opposed to being driven by an independent recurrent event. None of the missense mutations were found in genes that are known to be significantly ($q \leq 0.05$) mutated in human melanoma according to MutSig2CV analysis (Broad Institute TCGA Genome Data Analysis Center – 2016: Mutation Analysis; MutSig2CV v3.1). Nevertheless, in the cohort of human melanomas from TCGA ($n = 290$), 4 out of 14 orthologous genes were recurrently mutated and 8 harbored protein-inactivating mutations such as nonsense or splice-site mutations or frameshift deletions (Supplemental Table 2).

Recurrent CNAs in murine melanomas. To assess the role of chromosomal aberrations in $BRAF^{V600E}$- and $NRAS^{Q61K}$-driven melanomas, whole-genome shallow sequencing (WGSS) was performed and the landscape of somatic CNAs was established based on read depth. In total we sequenced 70 primary melanoma lesions (Figure 1 and Supplemental Table 1) derived from 35 $BRAF^{V600E}$- and 35 $NRAS^{Q61K}$-mutant mice. Among the $BRAF^{V600E}$-driven melanoma lesions, 7 were engineered to lack *Ink4a*, 6 had conditional deletion of *Pten* (14), 6 were knockouts for *Cdkn2a* locus, and 10 carried a $Trp53^{R172H}$ mutation frequently observed in UV-exposed human melanoma (19, 24). Of the $NRAS^{Q61K}$-driven lesions, 5 had deletion in *Ink4a*, 5 had deletion of the full *Cdkn2a* locus, and 16 carried conditional deletion in at least 1 of the *Trp53* alleles.

Chromosomal aberrations — both in terms of whole-chromosomal (broad) and focal CNAs — were significantly higher in $NRAS^{Q61K}$- than in $BRAF^{V600E}$-driven tumors (Supplemental Figure 2A). Nevertheless, GISTIC (https://software.broadinstitute.org/software/cprg/?q=node/31) identified recurrently deleted regions in $BRAF^{V600E}$-driven melanoma, encompassing well-established tumor-suppressor genes, including *Cdkn2a* and *Cdkn2b* (11%; $q = 1.76 \times 10^{-1}$) and *Pten* (26%; $q = 4.20 \times 10^{-2}$) as well as *Trp53* and *Nf1* (14%, $q = 3.40 \times 10^{-2}$; Figure 2, A–D, and Supplemental Table 3 for an overview of all recurrently deleted loci). Whereas chromosome 12 (harboring, among other tumor suppressors, *p27Kip1*) and chromosome 19 (harboring *Pten*) were significantly deleted (17%, $q = 2.80 \times 10^{-5}$ and 17%, $q = 2.80 \times 10^{-5}$, respectively), amplification of chromosome 6, which contains *Kras* and *c-Raf*, was frequently observed (23%, $q = 2.73 \times 10^{-9}$; Figure 2A).

In addition to few other recurrent focal CNAs (Supplemental Table 3), GISTIC identified 3 distinct regions located next to

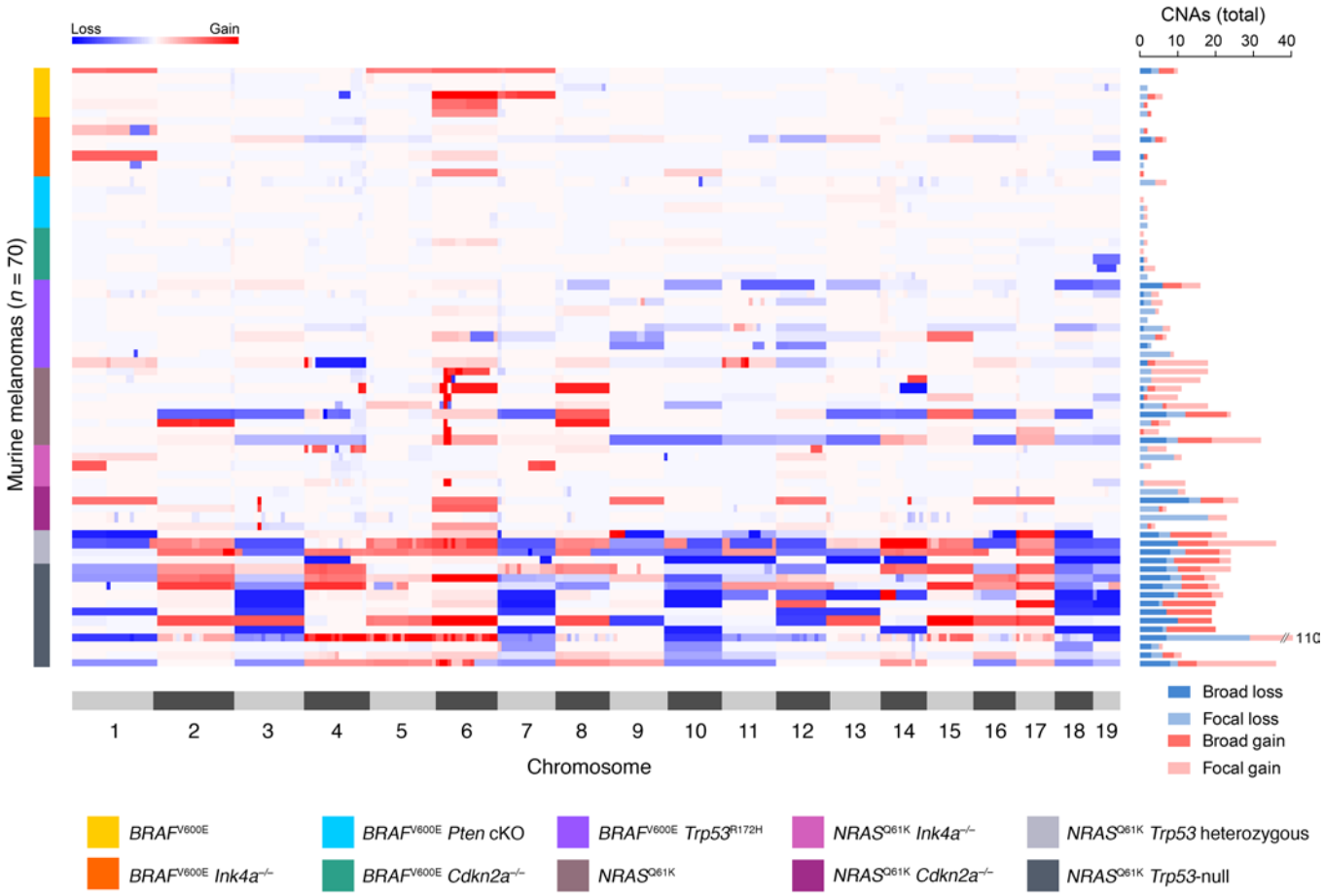

Figure 1. Landscape of CNAs in genetically induced murine melanomas. Heat map of CNAs in 70 $BRAF^{V600E}$- and $NRAS^{Q61K}$-driven murine melanomas. The genetic background of each sample is color coded based on the legend provided at the bottom of the panel. The copy-number gains and losses are depicted in red and blue, respectively. Chromosome numbers are shown on the *x* axis. The total number of CNAs (focal and broad) is shown on the right panel.

one another on chromosome 6, which are recurrently amplified in $NRAS^{Q61K}$-driven lesions (Figure 2, B and D, and Supplemental Table 3 and 4). One of these regions encompasses 31 genes, including *Braf* (68%, $q = 1.05 \times 10^{-16}$). The adjacent region contains 72 genes, including *Smo* (68%, $q = 5.50 \times 10^{-19}$), which encodes a key transducer of hedgehog (Hh) signaling (25), and the third region did not carry any known or predicted oncogenes. The *Braf*-containing region was no longer significantly amplified when all lesions, including the $BRAF^{V600E}$-driven melanoma, were included in GISTIC, indicating that this particular focal event specifically occurs on an $NRAS^{Q61K}$-mutant background. Notably, none of these 3 regions were amplified in $NRAS^{Q61K}$ lesions that carried inactivating mutations within the *Trp53* locus, indicating the loss of p53 alleviates the need for these focal amplification events. In contrast, 2 focal losses on chromosome 8 (13%, $q = 1.03 \times 10^{-1}$), encompassing a single gene (*Csmd1*), and chromosome 14 (25%, $q = 1.21 \times 10^{-2}$), encompassing 24 genes, were only observed in *Trp53*-null $NRAS^{Q61K}$ lesions (Figure 2C). Interestingly, *Csmd1* is a tumor suppressor frequently deleted and mutated in human melanoma and is commonly lost in many other tumor types (26). Overall, these data indicate that broad and focal CNAs are likely to influence the progression of $BRAF^{V600E}$- and $NRAS^{Q61K}$-driven tumors by affecting regions harboring established and novel putative cancer genes.

Whole-chromosome aberrations, and in particular losses (of chromosomes 1, 3, 7, 10, 11, 12, 18, and 19), were especially frequent in samples carrying conditional deletion in one or both *Trp53* alleles (Figure 1 and Figure 2C, Supplemental Figure 2C, Supplemental Figure 3A, and Supplemental Table 5). Importantly, quantitative reverse-transcriptase PCR (RT-qPCR) analysis revealed that *Trp53* mRNA levels in all *Trp53* heterozygous lesions were comparable to those seen in *Trp53*-null lesions, indicating that all 4 heterozygous lesions underwent *Trp53* loss of heterozygosity (LOH) (Supplemental Figure 4A). These data indicate that there is a selective pressure for p53 loss of function on this background and that p53 deficiency promotes aneuploidy in skin melanoma. A similar phenomenon was recently described for nonmelanoma skin cancer (23) and was also observed in mouse liver cancers in which the p53 pathway was functionally inactivated (Supplemental Figure 4B). Interestingly, comparing the results from GISTIC of different tumor types — including data from murine SCLCs (27) and cutaneous SCCs (23) — indicated that the recurrent broad alterations are cancer-type specific (Supplemental Figure 4C). For instance, whereas loss of chromosome 19 (harboring *Pten*) was commonly seen in all tumor types, except liver carcinoma, amplification of chromosome 4 or loss of chromosome 9 was a very frequent event only in mouse small cell lung cancers (mSCLCs) and

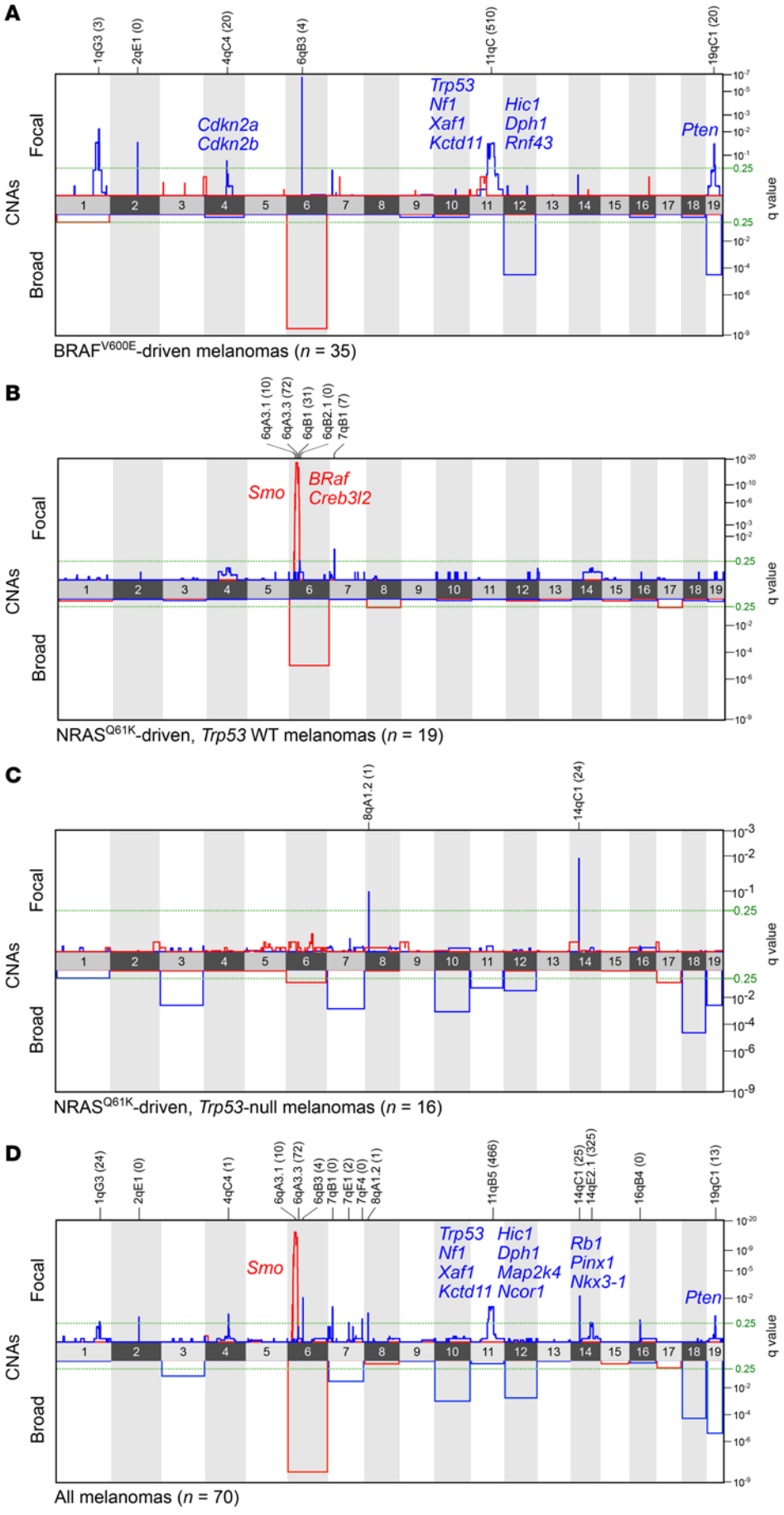

Figure 2. GISTIC analysis of recurrent genetic alterations in murine melanomas. Recurrent focal and whole-chromosomal amplification and deletion in BRAFV600E-driven lesions (**A**; *n* = 35); NRASQ61K-driven, Trp53 WT lesions (**B**; *n* = 19); NRASQ61K-driven, Trp53 heterozygous or homozygous null lesions (**C**; *n* = 16); and all samples combined (**D**; *n* = 70). Recurrent deletions and amplifications are shown in red and blue, respectively. The green dashed lines in all panels indicate the set significance threshold of 0.25. Genes of interest are listed next to focal gains and losses, and the numbers of protein-coding genes in the peak of the CNA are shown in parentheses.

Table 1. Comparative genomics identifies putative melanoma TSGs

Mouse gene	Human gene	TSG validated in GEMMs of melanoma	Significant association between RNA abundance and patient survival	Reference
Pten	*PTEN*	x	x	14
Cdkn2b	*CDKN2B*	x		31
Nf1	*NF1*	x		32
Stk11	*STK11 (LKB1)*	x		33
Trp53	*TP53*	x		19
Fes	*FES*		x	
Agap2	*AGAP2*		x	
Prdm1	*PRDM1 (BLIMP1)*		x	
Bcl10	*BCL10*		x	
Kctd11	*KCTD11*		x	
Nkx3-1	*NKX3-1*		x	
Rap1a	*RAP1A*		x	
Tnfaip3	*TNFAIP3 (A20)*		x	
Apc	*APC*			
Brms1	*BRMS1*			
Cadm4	*CADM4*			
Dph1	*DPH1 (OVCA1)*			
Hif3a	*HIF3A*			
Kank1	*KANK1*			
Lats1	*LATS1*			
Map2k4	*MAP2K4 (MKK4)*			
Mcc	*MCC*			
Men1	*MEN1*			
Ncor1	*NCOR1*			
Pdcd4	*PDCD4*			
Rb1	*RB1*			
Sash1	*SASH1*			
Smad2	*SMAD2*			
Smad4	*SMAD4*			
Sufu	*SUFU*			

nonmelanoma skin carcinomas, respectively. Similarly, recurrent loss of chromosome 10 was only observed in mouse melanoma.

Comparative genomics identifies putative melanoma drivers. GISTIC indicated that some of the focal and broad alterations described above occurred more frequently than expected by chance, suggesting that these events provide selective advantage during tumor progression and may therefore involve key cancer (and/or melanoma) genes. Importantly, these events are of potential clinical relevance in human melanoma, as a significant overlap between orthologous genes located on broad CNAs in human and murine melanoma was observed (Supplemental Figure 5, A–D). To begin cross-species analysis of human cancer and murine melanoma genomes, we compiled a list of genes located in chromosomal regions (both focal and broad CNAs) that are recurrently and specifically deleted in mouse melanoma lesions ($n = 5204$ genes) and searched for evidence of (epi)genetic alterations and/or deregulation of expression of their human orthologues in the melanoma clinical samples from the TCGA cohort (see Methods for a detailed description of the pipeline). 1250 orthologues exhibited (focal or broad) CN loss with significant association between CN and RNA abundance (FDR ≤ 0.01). Single-nucleotide alterations (SNAs) were identified in 17 genes, and the promoter region of 396 genes exhibited evidence of DNA hypermethylation, an epigenetic mark that typically associates with repression of transcription (28, 29). Importantly, 30 of these genes had already been enlisted into various tumor-suppressor gene (TSG) databases, including UniProt (http://www.uniprot.org/) and that referenced by Vogelstein et al. (Table 1 and Supplemental Table 6; ref. 30). Webgestalt (http://webgestalt.org/option.php), KEGG (http://www.genome.jp/kegg/genes.html), GeneSetDB (http://genesetdb.auckland.ac.nz/haeremai.html), and Ingenuity Pathway Analysis (IPA) (QIAGEN) revealed a significant enrichment in genes implicated in pathways known to play important roles in melanomagenesis such as TGF-β ($P_{adj} = 4.7 \times 10^{-5}$), Wnt/β-catenin ($P_{adj.} = 1.1 \times 10^{-5}$), the MAPK signaling pathway ($P_{adj.} = 5.5 \times 10^{-5}$), Hh ($P_{adj} = 2.4 \times 10^{-2}$) and p53 signaling ($P_{adj} = 1.3 \times 10^{-3}$), and biological processes regulating the cell cycle ($P_{adj.} = 2.0 \times 10^{-9}$), apoptosis ($P_{adj.} = 2.0 \times 10^{-9}$), and cell movement ($P_{adj.} = 3.0 \times 10^{-10}$). IPA also indicated that the majority of these genes (23 out of 30, 76%) have multiple biological functional connections, indicating that this list is enriched for alterations/mutations affecting functionally interacting proteins (Supplemental Figure 6 and Supplemental Table 7).

Strikingly, virtually all of the genes validated as tumor suppressors in the $BRAF^{V600E}$- and/or $NRAS^{Q61K}$-driven melanoma mouse models, namely *Pten*, *Cdkn2b*, *Nf1*, *Trp53*, and *Stk11*, were among the 30 selected genes (Table 1; ref. 14, 31–34). Sporadic mutations and/or downregulation of expression of *APC* (35) and *PDCD4* (36) in human melanoma have also been described. Interestingly, one of these genes was the well-established negative regulator of the Hh signaling pathway, *Sufu*. Notably, *Kctd11*, another negative modulator of this pathway, was present among the 30 putative melanoma TSGs that have not been previously linked to melanomagenesis (Table 1). These data, together with the identification of *Smo* in a focally and recurrently amplified region of the mouse melanoma genome (Figure 2B), indicate that increased Hh signaling may contribute to melanomagenesis.

Importantly, further in silico analysis of the RNA-sequencing (RNA-seq) data set from the melanoma TCGA cohort revealed significant clinical associations between the RNA abundance of 9 (out of 30) genes and patient survival ($P < 0.1$; Table 1 and Supplemental Table 6, ref. 37). Only one of these genes (i.e., *PTEN*) has been previously linked to melanoma. Together, these analyses identified a series of new likely drivers and progression pathways with clinical importance in human melanoma.

A tumor-suppressor function for FES in human melanoma. Given that the central aim of this study was the identification of new melanoma drivers with clinical relevance to the human disease, we focused our attention on the 8 above-described genes that have not been previously implicated in melanoma biology, namely *NKX3-1*, *PRDM1*, *AGAP2*, *TNFAIP3*, *FES*, *KCTD11*, *RAP1A*, and *BCL10*. Importantly, analysis of a microarray data set (38) identified *KCTD11*, *FES*, and *TNFAIP3* as the only 3 genes that — similarly to *PTEN* — exhibited average lower levels of expression in a series of melanoma cell lines compared with various normal human melanocyte cultures (Supplemental Figure 7A). Interestingly, only one of these genes (*FES*) showed a robust inverse correlation between RNA abundance and DNA methylation levels

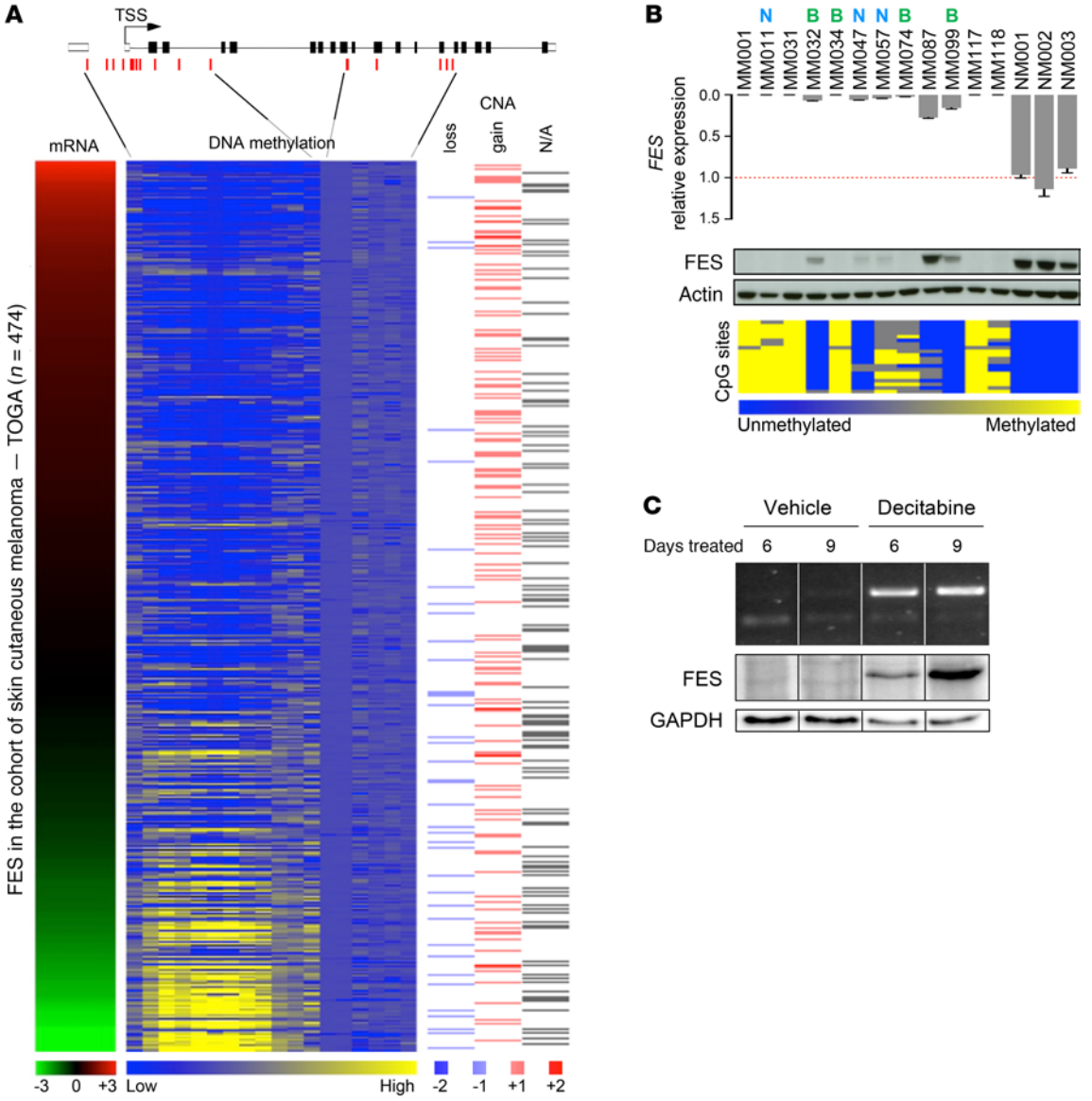

Figure 3. FES expression is regulated by promoter methylation in human melanomas. (**A**) Analysis of *FES* expression in 474 melanoma clinical samples from the TCGA cohort. The left panel shows *FES* mRNA levels ordered from the highest (red) to the lowest (green). The middle panel shows DNA methylation profile obtained from 19 array probes located in the CpG sites of *FES*. The schematic above shows a representation of the *FES* locus, with UTR regions in white and exons in black. CpG positions are shown as red stripes. The right panel depicts the copy number status of the *FES* locus split into cases that show loss (in blue) and gain (in red) and samples in which the CNA status of *FES* was not assessed (in gray). (**B**) FES expression in short-term melanoma cultures (MM) and 3 normal melanocyte cultures (NM). Upper graph shows expression of *FES* mRNA levels as determined by RT-qPCR. Values are normalized to the mean RNA level of normal melanocytes, which was set to 1. Error bars show mean ± SD (n = 2). The middle panel shows Western blot analysis of FES. Actin served as a loading control. The bottom panel shows methylation profile of short-term melanoma cultures and normal melanocytes as determined by bisulfite sequencing of 20 CpG sites located at positions ranging from –72 to +115 from the *FES*′ TSS. $BRAF^{V600E}$ (B) and $NRAS^{Q61K,L,R}$ (N) mutational status is indicated on top of the sample name. (**C**) Expression of FES in MM031 cell culture after treatment with demethylating agent decitabine or its vehicle. The upper panel shows *FES* mRNA levels assessed by qRT-PCR. Western blot analysis in the 2 lower panels shows FES protein levels. GAPDH served as a loading control.

in the vicinity of its transcription start site (TSS) (r = –0.7098, P < 0.0001; Supplemental Figure 7B). Importantly, whereas methylated CpG islands clustered at the 5′ end of *FES,* CpG islands located within the gene body were not methylated (Figure 3A). These data indicated that downregulation of *FES* expression in human melanoma may occur through a DNA methylation-dependent mechanism. Given that, in contrast to copy-number loss, epigenetic-dependent gene silencing can potentially be reversed using epigenetic drugs, we focused our attention on this particular putative TSG. Intriguingly, *FES* encodes a tyrosine kinase, a class of proteins best known for their potential protumorigenic, rather than tumor-suppressive, functions.

Further inspection of the RNA-seq data from the TCGA cohort revealed that *FES* expression levels were low (below the mean) in about 40% of these clinical samples (Figure 3A and Supplemental Figure 8A). Notably, there was no bias for any specific common

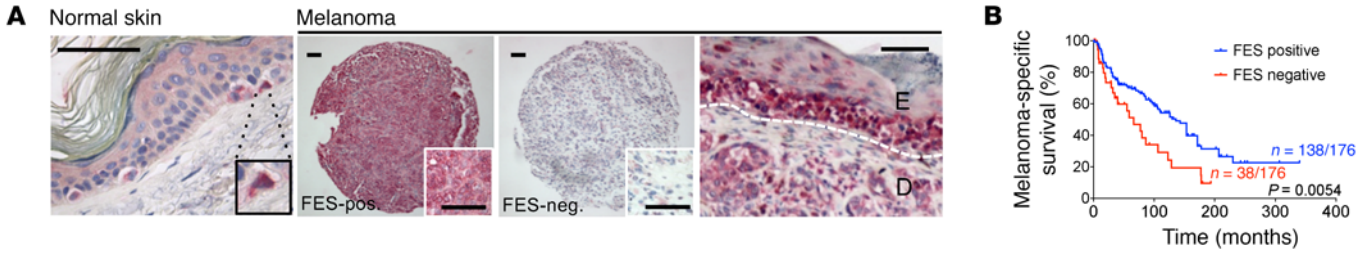

Figure 4. Low FES expression defines a subset of human melanoma with poor prognosis. (**A**) Representative pictures of FES staining in human cutaneous melanoma samples. Left panel shows FES staining in normal human skin; the inset shows a zoom-in view of a melanocyte residing in the basal layer of the epidermis. The three panels on the right show representative photographs of FES-positive and FES-negative melanoma cases. The photograph on the far right depicts the difference in the intensity of FES staining within melanoma. The epidermal layer (E) showed more intense staining compared with the dermal skin layer (D). Scale bars: 100 μm. (**B**) Kaplan-Meier curve of FES-positive versus FES-negative cases determined from FES staining on a tissue microarray containing 176 human metastatic melanoma samples. The survival time represents the time from the diagnosis of primary melanoma until the melanoma-related death of the patient. Statistical significance was determined by the Mantel-Cox test (α = 5.000%).

mutational event (i.e., BRAF versus NRAS mutations) to occur in these selected samples (Supplemental Figure 8B). Interestingly, low mRNA abundance significantly correlated with poor prognosis ($P = 0.0456$; Supplemental Figure 8C). To further validate and extend these results, we assessed *FES* mRNA levels by RT-qPCR in 8 normal human primary melanocyte cultures (NHME), 12 short-term melanoma cultures, and 23 melanoma cell lines (38). Whereas high levels of *FES* were detected in NHME cultures, *FES* mRNA levels were lower in most melanoma cultures (Figure 3B, Supplemental Figure 7A, and Supplemental Figure 8D). Western blotting analysis confirmed that the decrease in mRNA levels was correlated with a concomitant decrease in FES protein levels (Figure 3B and Supplemental Figure 8E).

To further confirm this finding, the CpG DNA methylation status of the region flanking the *FES*′ TSS was assessed by bisulfite sequencing in primary melanocytes and short-term (Figure 3B) and long-term (Supplemental Figure 8E) melanoma cultures. Little to no methylation was detected in primary melanocytes, which expressed high levels of *FES*. In contrast, the levels of CpG DNA methylation in human melanoma cultures were generally higher than in melanocytes and largely inversely correlated with *FES* mRNA abundance. Moreover, *FES* expression could be restored upon exposure of melanoma cells to 5-aza-2′-deoxycytidine (5-aza-dC, decitabine), which inhibits CpG methylation (Figure 3C).

Notably, in silico inspection of the human melanoma TCGA data indicated that the *FES* locus was not more frequently targeted by mutations than occurring by chance (MutSig 2CV, $q = 1$). Only a few missense mutations were identified (8 mutations from 278 patients from the TCGA cohort; 2.9%), and although 2 of these mutations affected residues located in the kinase domain (Supplemental Figure 8F), these residues were not conserved and the mutations are not predicted to affect the kinase activity, according to Meta-SNP (http://snps.biofold.org/meta-snp/) and PredictSNP2 (http://loschmidt.chemi.muni.cz/predictsnp2/; ref. 39). Together, these data indicate that cytosine methylation, rather than inactivating mutations, is a common mechanism of *FES* silencing in human melanoma.

The observation that *FES* is expressed in NHME was both new and, to some extent, surprising. Importantly, FES protein expression was readily detected by IHC in melanocytes from normal human skin, ruling out the possibility that the high levels of expression detected in NHME cultures was an artifact of in vitro culturing. Whereas FES expression was also elevated in all benign nevi examined, FES immunoreactivity varied from high/medium (FES positive) to very low/undetectable (FES negative) in various cutaneous melanoma samples included in an initial survey study (Figure 4A). Interestingly, in FES-positive samples, there was a tendency toward decreased immunoreactivity in the dermal invasive melanoma cells compared with the noninvasive epidermal component (Figure 4A). Consistently, an anticorrelation between *FES* mRNA levels and thickness according to Breslow (https://xenabrowser.net) was observed in the TCGA clinical samples (Supplemental Figure 8G).

To further survey FES protein expression in a larger cohort of biospecimens, 2 tissue micro-arrays (TMAs) from UZ Leuven (40) and 3 commercially available TMAs (ME1004d + ME2081 + ME2082b) containing collectively 27 benign nevi, 219 primary melanomas, and 221 metastatic melanomas were examined. The majority of nevi (85%) were positive for FES, whereas 39% of primary melanomas and 23% of metastatic melanomas expressed very low/undetectable FES levels. Two of the TMAs were annotated with survival outcomes and comprised 687 evaluable cores, corresponding to 176 melanomas, 40 of which were primary and 136 metastatic. Of the evaluable melanomas, 138 melanomas (75%) were positive (high/medium) and 38 (21%) were negative (low/undetectable) for FES. A statistically meaningful association was observed between FES protein levels and survival. Patients with low/undetectable levels of FES showed a significantly shorter survival than patients with high/medium FES protein expression (log-rank test: $P = 0.0054$, Figure 4B).

Importantly, whereas restoration of FES expression in 2 FES-negative melanoma cell lines (MeWo and 501 Mel) only minimally affected the proliferative capacity of these cells in optimal growth conditions, it did drastically decrease the ability of MeWo (and to a lesser extent 501 Mel) to form colonies when plated at low density and to support anchorage-independent growth in soft agar (Figure 5, A–C, and Supplemental Figure 9). Moreover, FES expression dramatically decreased the ability of MeWo to form tumors when injected into immune-compromised mice (Figure 5D). Importantly, FES-dependent growth inhibition was dependent on the integrity of its kinase domain, as reintroduction of

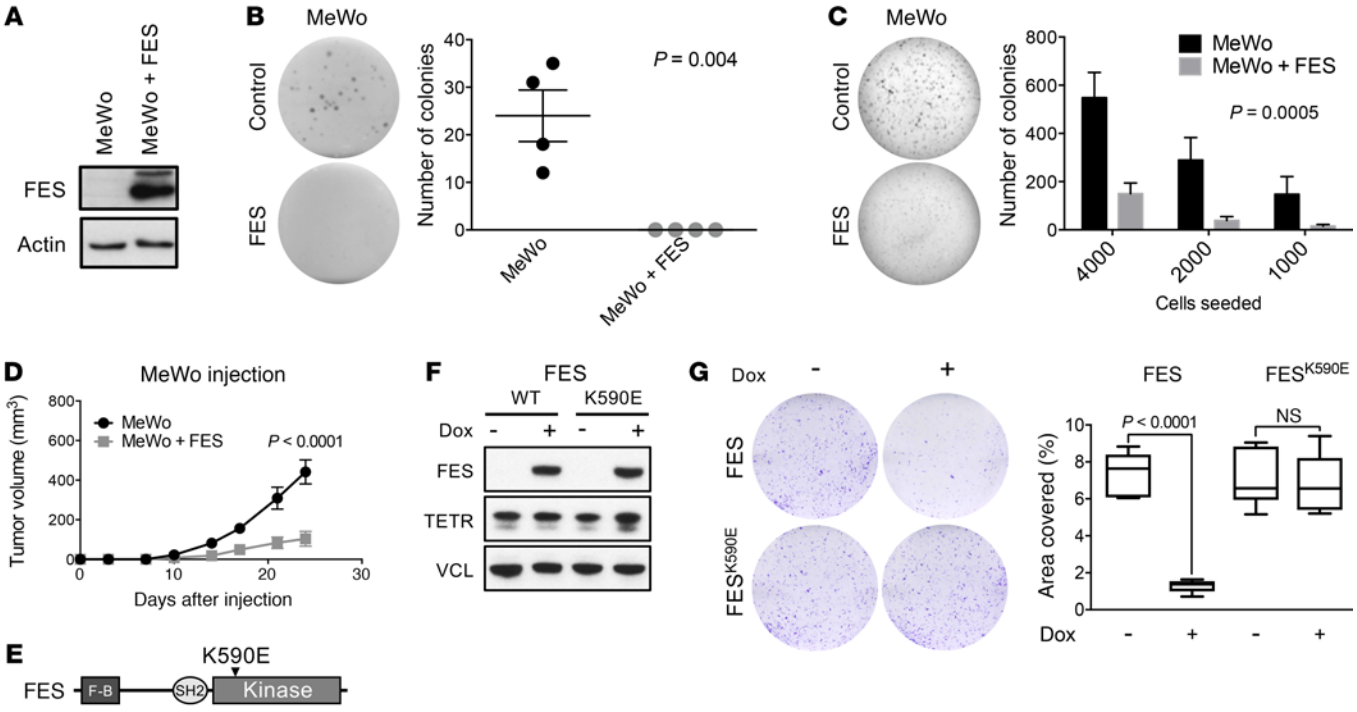

Figure 5. FES reexpression decreases cell proliferation in vitro and in vivo in a kinase-dependent manner. (**A**) Western blot analysis of FES in MeWo cell line with overexpression of FES. Actin served as a loading control. (**B**) Clonogenic assay of MeWo cells with and without expression of exogenous FES. Error bars indicate mean ± SEM (n = 4 biological replicates per group). (**C**) Soft agar assay of MeWo cells with and without expression of exogenous FES. Error bars indicate mean ± SEM (n = 3 biological replicates per group). (**D**) Mice (n = 9) were injected with 1×10^6 MeWo cells to the left or MeWo cells expressing exogenous FES to the right side of the body. The tumor volume was measured every 3 to 4 days up to day 24. Error bars indicate mean ± SEM (n = 9 biological replicates per group). (**E**) Schematic indicating the location of the FES kinase-dead mutation. F-B, F-BAR domain. (**F**) Western blot analysis of doxycycline-induced expression of WT or mutant FES in MeWo cell line. Vinculin served as a loading control. (**G**) Clonogenic assay of MeWo cells expressing WT or mutant FES. Quantification of the assay measured as the percentage of area covered is shown in the graph on the right. Error bars indicate mean ± SEM (n = 3 biological replicates per group). Statistical significance was determined by unpaired 2-sided t test (**B**, **G**) and 2-way ANOVA (**C**, **D**).

a FES kinase–dead mutant (K590E; ref. 41) did not affect the growth of MeWo melanoma cells (Figure 5, E–G). Together, these observations are consistent with a tumor-suppressor role for FES in human melanoma that depends on its kinase activity.

Fes deficiency promotes the progression of BRAF^{V600E}-induced murine melanoma. Together, the above data raise the possibility that FES may function as a tumor suppressor in melanoma. In order to directly test this possibility, we combined a *Fes*-null allele (42) with the *Tyr-Cre^{ERT2} Braf$^{CA/+}$* alleles. The *Braf$^{CA/+}$* allele enables tamoxifen-inducible expression of the constitutively active BRAF^{V600E} mutation. We initiated tumorigenesis in *Tyr-Cre$^{ERT2/°}$ Braf$^{CA/+}$ Pten$^{fl/fl}$ Fes$^{+/+}$* (*Fes* WT) and *Tyr-Cre$^{ERT2/°}$ Braf$^{CA/+}$ Pten$^{fl/fl}$ Fes$^{-/-}$* (*Fes* KO) animals by tamoxifen exposure on the back skin or tail. Macroscopic examination of the melanoma lesions after tumor induction revealed acceleration of tumor growth on the *Fes*-deficient background (Figure 6, A and B, and Supplemental Figure 10, A and B). Accordingly, *Fes* loss led to a significant reduction in tumor latency and significantly reduced overall survival (Figure 6C). Notably, *Fes* loss also led to a significant decrease in tumor latency and overall survival on the *Braf$^{CA/+}$ Ink4a$^{-/-}$* background, which is far less penetrant than the *Braf$^{CA/+}$ Pten$^{fl/fl}$* background (Figure 6D). Histological analyses confirmed that the dissected tumors were of melanocytic origin and stained positive for the melanoma marker S100 (Figure 6E and data not shown). A significant increase in the proliferation index and in the number of cells positive for the cell proliferation marker Ki67 in *Braf$^{CA/+}$ Pten$^{fl/fl}$ Fes* KO, as compared with WT, tumors (Figure 6, E and F) indicated that *Fes* loss drives tumor progression, at least in part, by promoting an increase in melanoma cell proliferation. Together, these data establish *Fes* as a suppressor of BRAF^{V600E}-driven melanomagenesis in mice.

To gain insights into the molecular mechanisms underlying Fes' tumor-suppressor function, we profiled the transcriptome of *Tyr-Cre$^{ERT2/°}$ Braf$^{CA/+}$ Pten$^{fl/fl}$ Fes$^{+/+}$* and *Tyr-Cre$^{ERT2/°}$ Braf$^{CA/+}$ Pten$^{fl/fl}$ Fes$^{-/-}$* melanoma lesions (n = 5 per group) by RNA-seq. Differential gene expression analysis showed enrichment for signatures associated with increased Wnt signaling ($P = 3.77 \times 10^{-3}$) and cell proliferation ($P = 7.51 \times 10^{-3}$) among the upregulated genes and immune response among the downregulated genes ($P = 3.51 \times 10^{-27}$; Figure 7, A and B, and Supplemental Table 8). Previous reports indicated that active β-catenin signaling in melanoma is associated with increased cell proliferation and more aggressive disease (17). Moreover, tumor-intrinsic β-catenin activation dominantly excludes T cell infiltration into the melanoma tumor microenvironment (43). An increase in β-catenin signaling may therefore, at least partly, drive both the increased cell proliferation gene expression signature and, indirectly, the downregulation of genes linked to immune response.

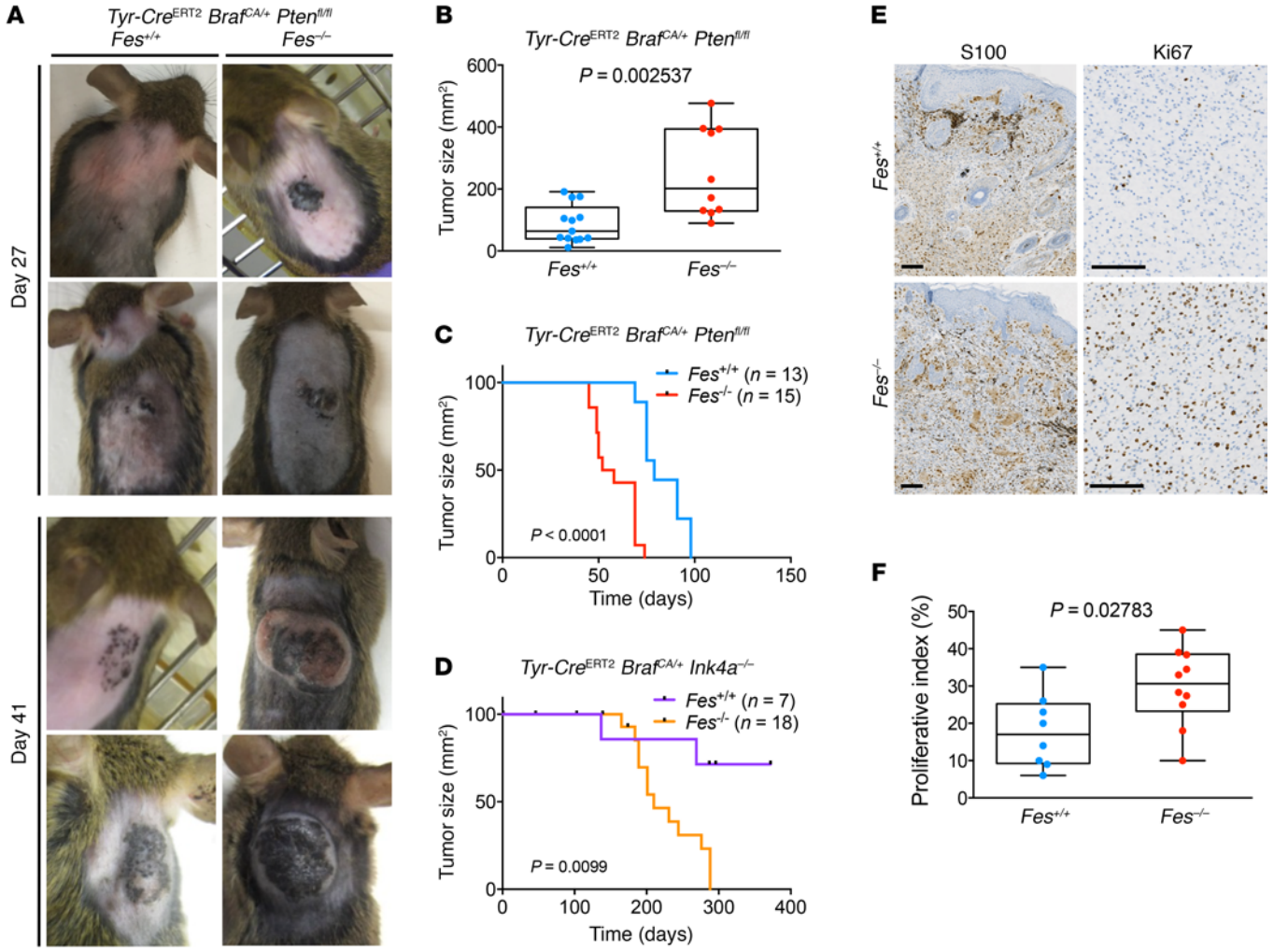

Figure 6. *Fes* loss accelerates progression of BRAF^{V600E}-driven, PTEN-deficient, or INK4a-deficient melanoma. (**A**) Representative photographs of *Tyr-Cre*^{ERT2} *Braf*$^{CA/+}$ *Pten*$^{fl/fl}$ mice either *Fes*$^{+/+}$ or *Fes*$^{-/-}$ at days 27 and 41 after topical treatment of the back skin with 5 mM 4-HT. (**B**) Box plot shows the tumor volume measured at day 40 after 4-HT exposure of *Fes*$^{+/+}$ (n = 13) or *Fes*$^{-/-}$ (n = 10). (**C**) Kaplan-Meier analysis of *Fes*$^{+/+}$ (n = 13) and *Fes*$^{-/-}$ (n = 15) mice on a *Tyr-Cre*^{ERT2} *Braf*$^{CA/+}$ *Pten*$^{fl/fl}$ background. (**D**) Kaplan-Meier analysis of *Fes*$^{+/+}$ (n = 7) and *Fes*$^{-/-}$ (n = 18) mice on a *Tyr-Cre*^{ERT2} *Braf*$^{CA/+}$ *Ink4a*$^{-/-}$ background. (**E**) IHC of S100 melanoma and Ki67 proliferation markers in *Tyr-Cre*^{ERT2} *Braf*$^{CA/+}$ *Pten*$^{fl/fl}$ melanomas that were WT or KO for *Fes*. Scale bars: 100 μm. (**F**) Proliferative index of *Fes*$^{+/+}$ (n = 8) or *Fes*$^{-/-}$ (n = 10) melanomas from **E** determined by counting Ki67$^+$ nuclei within the tumor. Statistical significance was determined using the Mann-Whitney U test (**B** and **F**) or the Mantel-Cox test (**C** and **D**). Box boundaries, 25th and 75th percentiles; whiskers, minimum and maximum; center line, median (**B** and **F**).

Total β-catenin protein levels were not significantly higher in *Fes* KO tumors. Similarly, mRNA expression levels of the gene encoding β-catenin (*Ctnnb1*) were not affected by *Fes* loss (Supplemental Figure 10C). Consistent with elevated β-catenin signaling, however, a clear accumulation of nuclear β-catenin was observed in *Fes*-deficient lesions (Figure 7, C–F). In contrast, levels of p-Erk, p-Akt (Ser-473), and p-STAT3 were comparable in *Fes* WT and KO melanoma lesions, indicating that MAPK, PI3K, and JAK-STAT signaling were, by and large, not affected by *Fes* loss (data not shown).

Expression of many melanocytic pigmentation genes is controlled by the melanocyte-specific isoform of melanogenesis-associated transcription factor (MITF), MITF-M, which is a downstream target of β-catenin signaling (44, 45). Enhanced β-catenin signaling in melanoma is therefore often accompanied by an MITF-M–dependent increase in melanocytic differentiation markers (17). Consistently, increased MITF-M protein levels and upregulation of MITF target genes, such as *Trp1*, *Trp2*, and *Tyr*, were observed in *Fes* KO melanoma lesions (Supplemental Figure 10, D and E). An increase in the cell differentiation gene expression signature ($P = 5.82 \times 10^{-3}$) was also apparent in the *Fes* KO lesions (Figure 7A). Finally, consistent with an increase in expression of melanocytic pigmentation genes, *Fes* KO melanoma lesions were more pigmented than their *Fes* WT counterparts (Supplemental Figure 10F and data not shown). Together, these results establish a clear genetic link between FES and melanoma progression and indicate that FES dampens tumor progression, at least in part, by decreasing β-catenin activation.

Discussion

Our study provides what we believe is the first comprehensive analysis of the genomic landscape of the widely used BRAF^{V600E}- and/or NRAS^{Q61K}-driven mouse models of melanoma. This analysis provides important insights into the biology of these geneti-

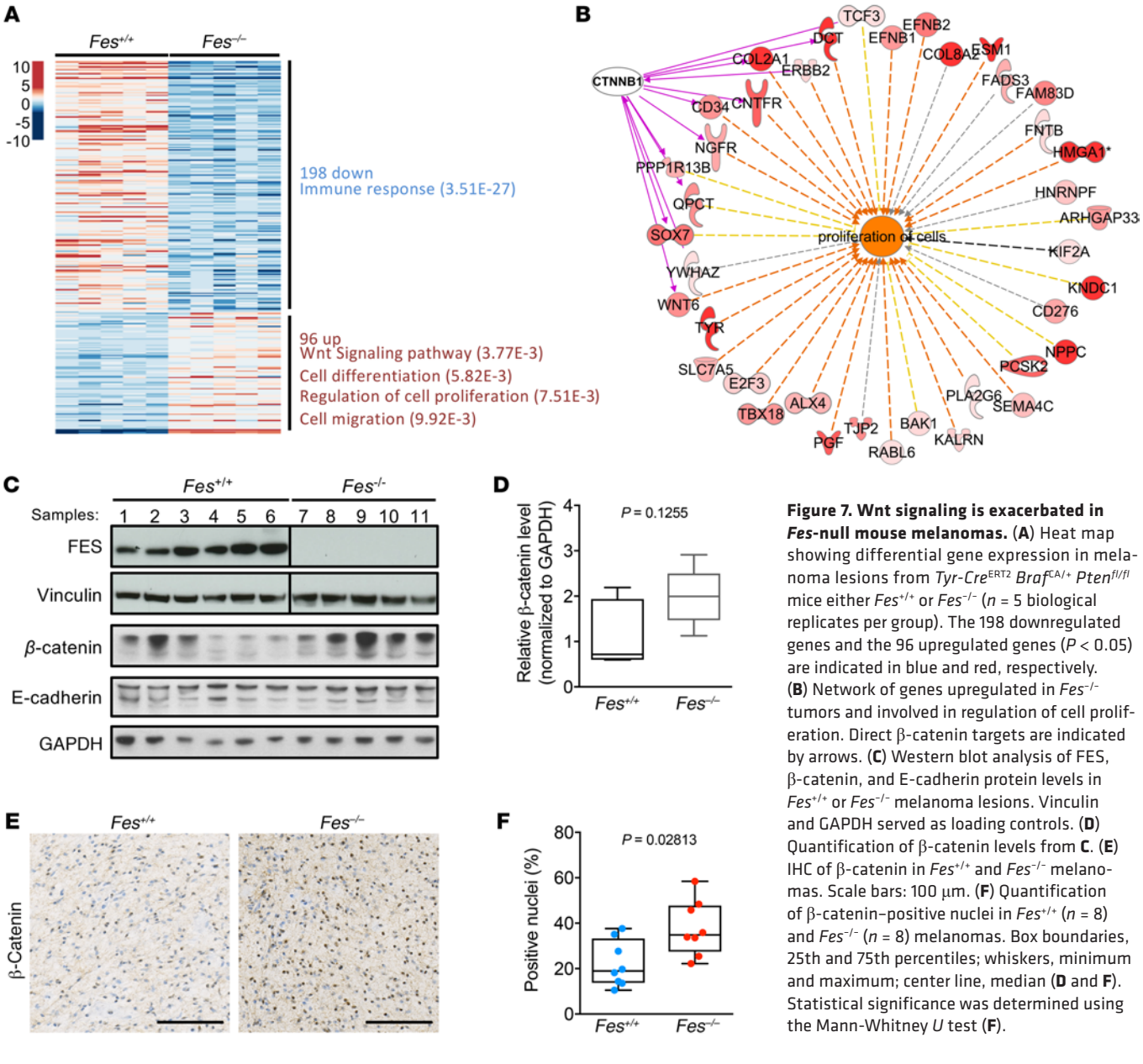

Figure 7. Wnt signaling is exacerbated in *Fes*-null mouse melanomas. (**A**) Heat map showing differential gene expression in melanoma lesions from *Tyr-Cre*^{ERT2} *Braf*$^{CA/+}$ *Pten*$^{fl/fl}$ mice either *Fes*$^{+/+}$ or *Fes*$^{-/-}$ (n = 5 biological replicates per group). The 198 downregulated genes and the 96 upregulated genes ($P < 0.05$) are indicated in blue and red, respectively. (**B**) Network of genes upregulated in *Fes*$^{-/-}$ tumors and involved in regulation of cell proliferation. Direct β-catenin targets are indicated by arrows. (**C**) Western blot analysis of FES, β-catenin, and E-cadherin protein levels in *Fes*$^{+/+}$ or *Fes*$^{-/-}$ melanoma lesions. Vinculin and GAPDH served as loading controls. (**D**) Quantification of β-catenin levels from **C**. (**E**) IHC of β-catenin in *Fes*$^{+/+}$ and *Fes*$^{-/-}$ melanomas. Scale bars: 100 μm. (**F**) Quantification of β-catenin–positive nuclei in *Fes*$^{+/+}$ (n = 8) and *Fes*$^{-/-}$ (n = 8) melanomas. Box boundaries, 25th and 75th percentiles; whiskers, minimum and maximum; center line, median (**D** and **F**). Statistical significance was determined using the Mann-Whitney U test (**F**).

cally engineered melanomas. Moreover, because of the reduced mutational noise compared with human melanoma, comparative genome analysis of these mouse lesions with their human counterparts and integration of these data with publically available epigenomic and transcriptomic data from human melanoma clinical samples allowed the identification of what we believe are previously unknown drivers of melanoma progression.

Our analysis reveals highly molded somatic melanoma mouse genomes with a very low somatic point mutation frequency and much fewer CNAs and structural rearrangements than their human counterparts. Notably, as previously observed in other p53-deficient mouse cancers, including lung (27), lymphoma (46), or nonmelanoma skin cancers (23), functional inactivation of p53 led to dramatic chromosomal rearrangements. Inactivation of p53 can therefore be used as a genetic trick to recapitulate the dramatic chromosomal rearrangements seen in human melanoma.

The majority of genomic alterations observed in the mouse lesions were focal and broad deletions, which are likely associated with loss of TSG function. This is only partly surprising, since the lesions were engineered to already express either one of the two most common melanoma oncogenes, namely BRAF^{V600E} and NRAS^{Q61K}. Focusing on the recurrently deleted regions, a list of 30 putative melanoma tumor suppressors has been established through comparative oncogenomics analysis. A striking observation is that a majority of these genes are highly functionally linked, which further supports the notion that melanoma therapies should be directed against signaling pathways themselves rather than individually mutated genes and provide a rational explanation as to why only transient therapeutic responses to BRAF^{V600E} inhibitors are observed in BRAF-mutated melanoma patients (12).

All melanoma TSGs validated genetically using mouse models, namely *Pten*, *Cdkn2b*, *Nf1*, *Trp53*, and *Stk11* (also known as

Lkb1), and several other genes previously linked to melanoma (i.e., *Apc*), were present in this list. Importantly, about 20 genes that have not been causally linked to melanoma were also identified, half of which have potential value in predicting human patient survival outcomes. This analysis therefore provides a rich resource of clinically relevant melanoma genes and a framework for further genomic validation of these genes as bona fide melanoma TSGs. In the context of the present study, we chose to validate one of these genes, *Fes*, by compound deletion in the autochthonous $BRAF^{V600E}$-driven mouse melanoma model. Importantly, we provide genetic evidence that inactivation of *Fes* promotes melanoma progression and decreases survival of animals bearing $BRAF^{V600E}$-expressing melanoma lesions. Together, these data illustrate the potential of this comparative and integrative genomic effort to identify acquired drivers of progression and dissect stepwise tumorigenesis.

FES was first described as the product of a viral oncogene (47) and has been implicated in growth and survival signaling in leukemia cell lines driven by oncogenic KIT and FLT3 receptors (48, 49). Despite these initial observations, there is to date no clear evidence that FES functions as an oncoprotein in human cancer. In contrast, large-scale sequencing of the tyrosine kinome in colorectal tumors identified *FES* as one of a few mutated genes (50). Although not conclusive, the loss-of-function nature of these mutations and in vitro assays using colorectal cancer cell lines raised the possibility that FES may instead function as a potential tumor suppressor (41, 51). Herein we provide clear evidence that *FES* functions as a TSG in both human and mouse melanoma. Consistent with this finding, an old study reported low levels of *FES* in a few human melanoma cell lines (52).

Protein kinases are often upregulated in cancer and are attractive therapeutic targets. However, protein kinases exert pleiotropic functions, such as increased survival, progression of the cell cycle, differentiation, adherence, or migration, that are dependent on the tissue and molecular environment of the cells. Ultimately, this implies a context-dependent functional role of specific kinases in cancer, i.e., oncogene or TSG function (53). Our data provide an additional example of a tyrosine kinase that acts as a tumor suppressor. Importantly, kinase inhibitors are now widely used in the clinic, including for the treatment of melanoma. Despite assertions on selectivity, most available inhibitors target multiple protein kinases in addition to the intended target (54). Considering the increasing list of kinases with putative TSG function, a comprehensive characterization of protein kinase function and kinase inhibitor selectivity profiling is essential for the proper management of these drugs in the clinic. Of note, FES is inhibited by ALK inhibitors (55) and several FDA-approved drugs such as the CDK1/2 inhibitor III, sunitinib, or bosutinib (56).

Whereas nuclear β-catenin, which reflects canonical Wnt pathway activation, is present in about 30% of human melanoma specimens (57), β-catenin-stabilizing mutations are only found in about 5% of the cases (43, 58, 59). The molecular mechanisms underlying such a frequent dysregulation of β-catenin localization and activation of function remain unclear (60). Interestingly, our data raise the possibility that epigenetic downregulation of *FES* transcription is one key mechanism that contributes to Wnt signaling activation in β-catenin WT melanomas. Our transcriptomic analysis indeed indicated that FES may function as a Wnt pathway inhibitor and, consistently, an increase in nuclear β-catenin levels was observed in *Fes*-deficient $BRAF^{V600E}$-driven tumors. This observation is in line with the previously reported cooperativity between stabilized β-catenin and $BRAF^{V600E}$ in the formation of aggressive mouse melanomas (17). Note that since stabilized β-catenin also cooperates with activated NRAS in mouse melanoma development (61), it is possible and may be likely that loss of *Fes* may also accelerate melanomagenesis on the NRAS-mutant background; this remains to be tested experimentally. We also show herein that ectopic FES expression severely compromised the in vitro and in vivo growth of MeWo cells, which express WT β-catenin. In contrast, FES-induced growth inhibition was far less dramatic in 501 Mel cells, which carry a β-catenin-stabilizing mutation (59). Taken together, these data indicate that FES exerts its tumor-suppression function, at least partly, as an inhibitor of canonical WNT–β-catenin signaling. Although the molecular mechanism underlying FES-dependent inhibition of WNT signaling remains to be fully elucidated, our data indicate that FES modulates β-catenin cellular localization, rather than its stability, in a manner that depends on its kinase activity. Additional work is needed to determine whether FES affects β-catenin nuclear translocation indirectly or directly, by phosphorylating β-catenin itself.

Recurrent focal and broad amplifications in the mouse melanoma genomes were not as common as recurrent deletions. Broad amplifications of chromosome 6 were nevertheless significantly ($q \leq 0.25$) recurrent in both $BRAF^{V600E}$- and $NRAS^{Q61K}$-driven melanomas. In addition, 3 distinct recurrent focal amplifications, all located on chromosome 6, were also observed in $NRAS^{Q61K}$-driven melanomas. Notably, one of them contained the *Braf* gene, which indicates that increased *Braf* expression may promote a growth advantage to $NRAS^{Q61K}$-driven melanoma lesions. Interestingly, one of these recurrent amplifications contained *Smo*, a key signal transducer of Hh signaling. This observation raises the possibility that increased Hh signaling may contribute to melanomagenesis. Consistent with this possibility, several components of Hh signaling pathway, including the well-established negative regulators *Sufu* and *Kctd11*, are among the 30 melanoma TSGs we identified. To date, only few studies have tentatively implicated Hh signaling in melanoma (62–64). Our work therefore warrants further dissection of the role of Hh signaling in melanomagenesis and leads us to entertain the possibility that Hh inhibitors should be considered in the context of (combination) melanoma targeted therapies.

This work provides a rich resource of candidate genes involved in melanoma progression in addition to a list of pathways and biological processes with potential clinical importance in the treatment of human melanoma.

Methods

Transgenic mice. The *Tyr-Cre*$^{ERT2/°}$, *Braf*$^{CA/+}$, *Braf*$^{LSL\text{-}V600E/+}$, *Ink4a*$^{-/-}$, *Pten*$^{fl/fl}$, *Tyr-Nras*$^{Q61K/°}$, *Trp53*$^{-/-}$, *Trp53*$^{fl/fl}$, *Cdkn2a*$^{-/-}$, *R26R*$^{LSL\text{-}eYFP/+}$, and *Fes*$^{-/-}$ mouse lines and strategies used for genotyping these mice were described previously (13, 21, 22, 42, 65–71). The various cohorts of compound mice were on mixed genetic backgrounds consisting of more than 85% C57BL/6J and, to a lesser extent, 129SvJ and FVB. The full list of samples collected from the compound mice and their genetic background can be found in Supplemental Table 1.

Activation of the Tyr-Cre^{ERT2} locus. Topical administration of 4-hydroxytamoxifen (4-HT) was conducted by preparing a 50 mg/ml solution (130 mM) of 4-HT (70% Z-isomer, Sigma-Aldrich) in DMSO. For localized melanoma induction on the back, 3- to 4-week-old mice were anesthetized and depilated on a 2-cm^2 patch of skin on the back with a combination of gum rosin and beeswax (Sigma-Aldrich). After the area was dried and cleaned, 1 μl of 5 mM 4-HT in ethanol vehicle was applied using a pipette. For distal tail inductions, 4 μl of 130 mM 4-HT was applied on the middle part of the tail (4 cm long) and wrapped by surgery tape to prevent the spread of 4-HT. The mice were evaluated weekly for tumor appearance and progression and measured with a caliper. The volume was calculated using the following formula: V = (length × width × height)/2. Mice were killed as soon as the tumors reached 15 mm^3 or sooner if they were suffering from tumor burden. Tumors and organs were snap-frozen in liquid nitrogen for further analysis or fixed in 4% paraformaldehyde, processed, and embedded in paraffin for histological studies.

Histology and IHC. Tissues were fixed overnight in 4% paraformaldehyde, dehydrated, paraffin embedded, sectioned (5 μm), and stained with H&E. For IHC, slides were stained with antibodies against S100 (Z0311; 1:300; Dako) and Ki67 (RM-9106-S; 1:200; ThermoScientific) and β-catenin (#9582; 1:1000; Cell Signaling Technology). Stainings were realized in the Ventana automated stainer from Roche using EnVision+ HRP reagent and DAB (DAB Peroxidase Substrate Kit, SK-4100; Vector Laboratories) for revelation. To assess proliferative index, Ki67-positive and -negative nuclei were counted in at least 3 microscopic fields randomly selected from different regions of each tumor section by applying a digital image analysis algorithm created on the ImageJ software platform (NIH). Proliferative index was then expressed as the ratio between positive and total numbers of nuclei. The percentages of β-catenin–positive nuclei were counted using ImageJ within 30 different fields from 8 different tumors per group.

IHC for FES was performed on formalin-fixed, paraffin-embedded material of benign nevi, primary and metastatic human melanomas, and TMA cohorts on the Leica BOND-MAX automatic immunostainer (Leica Microsystems) using primary antibody HPA001376 (1/100 dilution; Sigma-Aldrich). Antigen retrieval was performed onboard using a citrate-based buffer (Bond Epitope Retrieval Solution 1, pH 6.0; Leica) according to the manufacturer's instructions. Alkaline phosphatase activity was detected with Bond Polymer Refine Red Detection (Leica) as substrate, resulting in pink/red immunoreactivity. TMAs stained for FES were scored semiquantitatively by two researchers (FES negative, cores with melanoma cells showing low-intensity to undetectable cytoplasmic immunoreactivity; FES positive, cores with melanoma cells showing high- to medium-intensity cytoplasmic immunoreactivity; see Figure 4A for representative cores). Melanoma-specific survival was defined as the interval from diagnosis of the primary tumor to death from melanoma or date of last follow-up.

Cell culture. Melanoma cell lines (ATCC; ref. 72, 73) and Phoenix A cells (ATCC) were maintained in DMEM (Thermo Scientific) supplemented with 10% fetal bovine serum (Eurobio) and 2 mM glutamine (Thermo Scientific). Short-term melanoma cultures were maintained in Ham's F10 Nutrient Mix (Thermo Scientific) supplemented with 10% FBS and 4 mM glutamine. Cells were cultured in a 37 °C and 5% CO_2 incubator.

For the decitabine experiment, a final concentration of 0.5 μM decitabine (Sigma-Aldrich) was added to the cells and media were renewed every 3 days. After 6 or 9 days, cells were collected for RT-PCR and Western blot analysis.

For FES reexpression experiments, control or *Fes* cDNA LXSN retroviral vectors were transfected in Phoenix A cells using Lipofectamine 2000 (Thermo Scientific). Culture supernatants containing the retroviruses were used to infect melanoma cells in the presence of polybrene (Sigma-Aldrich) at 8 μg/ml overnight. After 2 rounds of infection, cells were selected using Geneticin (Thermo Scientific) at 1 mg/ml. For the clonogenic assay, 501 Mel or MeWo cells were seeded at low density in 60-mm culture plates in 3 ml media and grown for 8 to 10 days. Colonies were then fixed in 4% paraformaldehyde (Thermo Scientific), stained with 0.05% crystal violet, and counted. For the soft agar assay, cells were seeded in 12-well culture plates in 1 ml of supplemented DMEM containing 0.3% agar (Thermo Scientific). After 14 days, cells were stained with 0.002% crystal violet (Sigma-Aldrich) and colonies were scored using ImageJ software.

For the doxycycline-inducible expression of WT and kinase-dead mutant FES, MeWo cells were transduced with the lentivirus carrying the vector for TetR (FUGW plasmid with GFP replaced by TetR-T2A-NeomycinR) and selected with Geneticin (InvivoGen) at 1 mg/ml. Selected cells were transduced with lentivirus carrying a doxycycline-inducible conditional vector for FES^{WT} or FES^{K590E} and selected with puromycin (Sigma-Aldrich). The conditional vectors were made by Gateway-recombining pENTRY-FES$^{WT/K590E}$ vectors (41) with a pLENTI CMV/TO Puro DEST (Addgene, vector #17293). For the clonogenic assay, cells were plated onto 6-well plates at a density of 5,000 cells and incubated with doxycycline to induce the expression of FES. After 10 to 11 days, colonies were fixed and stained in a solution of 1% crystal violet in 35% methanol for 15 minutes and scored using ImageJ software.

MeWo cells injections. MeWo cells (1 million) were injected in 150 μl of 0.9% NaCl subcutaneously into nude mice (Janvier). Control and FES MeWo transfected cells were injected in the opposite flanks of mice. Tumor growth was monitored twice a week until week 24.

Bisulfite sequencing. Genomic DNA was extracted using the QIAamp DNA Mini Kit (QIAGEN). For bisulfite conversion, we used the EZ DNA Methylation Gold Kit (Proteigene) according to the manufacturer's instructions. Then a first PCR amplification was done (F-GTTGGGTTATTTTTTTTCGGTT and R-TAAATAAATCTCTAACCCTC), followed by a nested PCR (F-GGAGTAGGGGGGTTGGTAGG and R-CCTACTCTACCCCTACCTACC). PCR products were sequenced using the BigDye Terminator v1.1 Cycle Sequencing Kit (Thermo Scientific) on an Applied Biosystems 3130 DNA Analyzer.

Lysates and Western blotting. Cultured cells were lysed at 4°C in HNTG buffer (50 mM Hepes, pH 7.0, 150 mM NaCl, 1% Triton X-100, 10% glycerol, 1 mM EGTA, 1.5 mM $MgCl_2$) supplemented with protease inhibitor cocktail (Roche) and orthovanadate (Sigma-Aldrich). Protein concentrations were assessed using the Bradford protein assay (Bio-Rad). Following SDS-PAGE, lysates were transferred on PVDF membranes (Millipore). Immunoblotting was performed using rabbit polyclonal anti-ERK2 (Santa Cruz Biotechnology Inc.), mouse monoclonal anti–β-actin (Sigma-Aldrich), and rat monoclonal anti-Fes (Calbiochem) antibodies and SuperSignal West Pico Chemiluminescent Substrate (Thermo Scientific).

Tissue samples were additionally homogenized with Precellys Homogenizer (Bertin Technologies) in protein lysis buffer (25 mM HEPES, pH 7.5, 0.3 M NaCl, 1.5 mM $MgCl_2$, 2 mM EDTA, 2 mM EGTA, 1 mM DTT, 1% Triton X-100, 10% glycerol, phosphatase/protease

inhibitor cocktail); the extracts were incubated on ice for 15 minutes and centrifuged for 15 minutes in 4°C at 20,000 *g*. Protein concentration was measured by Bradford quantification and run on 4% to 12% NuPAGE Novex Bis-Tris Gels (Thermo Fisher Scientific). Membrane blocking (5% milk in TBS, 0.2%Tween-20) was followed by incubation with the appropriate primary antibodies and HRP-conjugated secondary antibody (Cell Signaling Technology). Proteins were detected by ECL and Western blotting (Thermo Scientific). Antibodies used are listed in Supplemental Table 9.

RT-qPCR. To extract RNA, samples were lysed in QIAzol (QIAGEN). Tumor samples were additionally homogenized with a Precellys Homogenizer (Bertin Technologies). RNA extraction was performed with the mRNeasy Mini Kit according to the manufacturer's instructions (QIAGEN). RNA was quantified using a NanoDrop 1000 (Thermo Scientific), and 2,000 ng was reverse transcribed with the High-Capacity cDNA Reverse Transcription Kit (Life Technologies). The results shown in Figure 3B were obtained by RT-qPCR reaction on an Applied Biosystems 7500 Fast Real-Time PCR System using SYBR Green PCR Master Mix (Thermo Scientific). Threshold cycle (Ct) values for Fes were normalized to housekeeping gene using the 2ΔCt formula. The results shown in Supplemental Figure 4A and Supplemental Figure 10, C and E, were obtained by RT-qPCR reaction on a Roche LightCycler 384 (Life Technologies) using Fast SYBR Green Master Mix (Life Technologies). Data were processed with qbase+ 2.6 software (Biogazelle) using a normalization method with a minimum of 2 reference genes. RT-qPCR primers are listed in Supplemental Table 10; the reference genes are indicated in the table as RefGen.

Epidermal whole mount. The epidermal whole mount was performed using an adaptation of a previously described protocol (74). Murine tail skin was dissected and spread out on Whatman cellulose filter paper. Pieces of murine tail skin were cut and incubated in 20 mM EDTA in PBS at 37°C for 40 minutes in the dark and subsequently washed twice with PBS. The epidermis was mechanically separated from the dermis as an intact sheet and was fixed in 4% paraformaldehyde for 30 minutes at room temperature in the dark. Pieces of epidermis were rinsed twice with PBS and stored at 4°C or immediately processed for antibody staining. For the staining, pieces of epidermis were incubated in blocking buffer (1% BSA, 10% donkey serum, 0.2% Tween in PBS) for 3 hours at room temperature on a rocking plate (120 rpm) in the dark. Blocked samples were incubated in primary antibodies diluted in antibody diluent (1% BSA, 0.2% Tween in PBS) overnight at 4°C in the dark. The primary antibodies used were anti-melanoma gp100 (rabbit, 1:400, Abcam, ab137078). Samples were then washed 3 times in PBS with 0.2% Tween for 1 hour and incubated in appropriate secondary antibodies diluted 1:1000 in antibody diluent for 2 hours at room temperature on a rocking plate in the dark. Nuclei were stained with DAPI solution (0.5 mg/ml) diluted 1:1,000 in PBS for 20 minutes and mounted in VECTASHIELD Antifade Mounting Medium for fluorescence (VECTOR).

Tissue collection, DNA extraction, and library preparation. In total, 70 mouse melanomas were collected for this study. The RNA/DNA from these lesions was extracted using the AllPrep RNA/DNA Kit (QIAGEN) or the DNeasy Blood & Tissue Kit (QIAGEN) following the manufacturer's instructions. The DNA samples from *Trp53*$^{LSL\text{-}R172H/+}$ *Braf*$^{LSL\text{-}V600E/+}$ *Tyr-Cre*$^{ERT2/°}$ tumors (n = 10) and *Braf*$^{LSL\text{-}V600E/+}$ *Tyr-Cre*$^{ERT2/°}$ tumors (n = 3) were provided by Richard Marais (Cancer Research UK Manchester Institute, Manchester, United Kingdom; ref. 24). DNA samples from *Nras*^{Q61K} *Cdkn2a*$^{-/-}$ melanomas (n = 5) were obtained from cells after tumor dissociation followed by initial expansion in nude mice and were provided by Lukas Sommer (University of Zurich, Zurich, Switzerland). Whole-genome DNA libraries were prepared using the KAPA HTP Library Preparation Kit (Kapa Biosystems) and either used for low-coverage whole-genome sequencing directly or further prepared for use in exome sequencing.

Exome sequencing, variant calling, validation, and scoring. In order to perform exome capture, the amplified DNA libraries were hybridized to a complete set of biotinylated long oligonucleotide probes using the SeqCap EZ Library Kit (Roche NimbleGen) for approximately 65 hours. After this, the exome-enriched libraries were washed and recovered using capture beads. The libraries were sequenced on a HiSeq2000 (Illumina) sequencing platform. An existing, in-house–developed pipeline for the analysis and annotation of somatic mutations in these samples was used (described below). Raw reads were mapped to the mouse reference genome (GRCm38/mm10) using the Burrows-Wheeler Aligner (v0.5.8a; ref. 75). Duplicate reads were marked using Picard (v1.43). We obtained an average coverage of 62× with on average 94% of the exome covered at least 10×. The Genome Analysis Toolkit (GATK; v2.1-13; Broad Institute; ref. 76) was used to recalibrate base qualities and local realignment around indels. Variant calling was performed using GATK's Unified Genotyper (GATK, v2.1-13). Small insertions and deletions of less than 50 bp were identified using Dindel (v1.01; ref. 77). Variants were functionally annotated using ANNOVAR (v2013Jun21; ref. 78). Somatic variant identification was performed by comparing tumor genomes with variants present either in the matching or combined normal samples. SNPs and indels reported by the Mouse Genome Project of the Sanger Institute were removed as well, according to the mixed genetic background of our mice. Mutations that were represented with more than 5% alternative reads in the control samples or mutations represented with less than 10% alternative reads in tumor samples were discarded. Resulting variants were manually inspected using the Integrative Genomics Viewer (IGV; v2.3.67; Broad Institute) in order to omit the variants in regions with low mapping quality and variants present but not called in the germline samples. Selected mutations were validated using Sequenom MassARRAY (Sequenom Inc.) genotyping according to the manufacturer's instructions. Primers were designed with MassARRAY Assay Design software v3.1. Automated genotyping calls were generated with MassARRAY RTTM software v4.0 and were validated by manual review of the raw mass spectra. Raw data were deposited in the ArrayExpress database (www.ebi.ac.uk/arrayexpress; E-MTAB-4917).

CNA analysis. For the analysis of CNAs, we performed low-coverage whole-genome sequencing of all 70 mouse melanomas on the HiSeq2500 (Illumina) sequencing platform. The sequencing reads were mapped to the reference genome (GRCm38/mm10) using the Burrows-Wheeler Aligner (v0.5.8a). The duplicate reads were removed using Picard (v1.43). After this, the mapped reads were binned in 30-kb windows and corrected for genomic waves using the PennCNV software package (79). The read counts per bin were transformed into logR values, and the data were segmented using ASCAT (80). logR values above 0.1 or below –0.1 were considered as amplified or deleted, respectively. The recurrent CNAs were identified using the GISTIC 2.0 tool (81). The control samples (n = 9) were used to filter out nonsomatic aberrations. Raw data were deposited in the ArrayExpress database (E-MTAB-4921).

RNA sequencing. RNA was extracted from *Tyr-Cre*$^{ERT2/°}$ *Braf*$^{CA/+}$ *Pten*$^{fl/fl}$ *Fes*$^{+/+}$ (*Fes* WT) and *Tyr-Cre*$^{ERT2/°}$ *Braf*$^{CA/+}$ *Pten*$^{fl/fl}$ *Fes*$^{-/-}$ (*Fes* KO) (n = 5 per group) melanomas using the RNeasy Mini Kit (QIAGEN) following the manufacturer's instructions. RNA integrity was assessed using Bioanalyzer 2100 (Agilent) and RNAs with RIN values of more than 7 were used for library preparation. RNA libraries were prepared using the Illumina TruSeq Stranded mRNA Sample Prep Kit (protocol 15031047, Rev E, October 2013). Illumina's NextSeq library Prep Kit (Illumina) was used to prepare the library from 1000 ng of RNA and the library quality was monitored on an HS DNA chip (Bioanalyzer, Agilent). Sequence libraries of each sample were equimolarly pooled and sequenced on a 0.5 run on the Illumina NextSeq 500 platform (high output, 75 bp, SR) generating on average 19.8 million reads per sample. FastQC was used to assess the quality of the sequenced data. Raw reads were mapped to the mouse reference genome (GRCm38/mm10) using STAR (version 2.51b) resulting in 66.0%–71.2% (13.2 to 16.6 million) of successfully mapped reads. Reads were assigned to Ensembl genes (GRCm38.84) and counted using the Subread package (version 1.4.6). Reads were normalized by size factors and $\log_2$. Differential expression analysis (*Fes* KO versus *Fes* WT) was performed using DESeq2 (version 1.10.1), and the GO enrichment analysis was performed using GOrilla (http://cbl-gorilla.cs.technion.ac.il; accessed July 2016). All original microarray data were deposited in the NCBI's Gene Expression Omnibus (GEO GSE83580).

Cross-species comparisons. To analyze the significance of overlap between genes located on broad CNAs in human and mouse (NRAS driven, *Trp53* null) melanomas, we explored the orthologous genes (Ensemble; accessed July 2016; total number of 1-to-1 orthologues 16,728) located on the significantly recurrent broad CNAs in human melanomas from the TCGA cohort (Broad Institute; v2016) and mouse melanomas from the NRAS-driven, *Trp53*-null cohort analyzed in this study. The comparison between gene expression and patient survival was performed by the online tool developed by Phil Cheng (University of Zurich, Switzerland; accessed March 2016; ref. 37), selecting only the metastatic melanoma samples and the 15th percentile as a cut-off for high and low expressers.

For the cross-species comparison of deleted genes, focal and broad deletions from all melanoma sample groups were intersected with orthologous genes targeted in human melanoma samples (TCGA repository). Only genes targeted in human melanomas by significantly recurrent deletions, mutations, or promoter hypermethylations were used for the analysis. Data (level 4) on CNAs in human melanomas were retrieved from the GDAC (Broad Institute TCGA Genome Data Analysis Center [2016]: SNP6 copy number analysis [GISTIC2.0]; Broad Institute of MIT and Harvard; doi:10.7908/C1445KXQ) performed on 367 samples. Genes targeted by CNAs in human melanomas and significantly positively correlating with the RNA levels ($q \leq 0.01$) were used for the cross-species comparison. Data on SNAs in human melanomas were retrieved from the MutSigCV analysis performed on 318 melanoma samples form TCGA (16). The data on DNA methylation from 476 human melanoma samples were obtained from the Xena repository (methylation 450 k; version 2015-10-26; http://xena.ucsc.edu/). CpG probes located 2 kb upstream or 500 bp downstream from the gene promoter were analyzed for hypermethylation. Probes showing more than 70% methylation in more than 10% of melanomas while having less than 25% methylation in the skin control samples were considered as hypermethylated.

Statistics. Group results were compared using unpaired two-sided t test. The statistical significance between the survival of two groups was determined by Mantel-Cox test. Mann-Whitney U-test was used when comparing groups with different distributions. Two-way ANOVA with Šidák method was used for multiple comparison analysis. Statistical significance of overlapping gene sets was determined using hypergeometric distribution test. Significance of correlation was determined using Pearson correlation coefficient test. Unless otherwise specified, a P value lower than 0.05 was considered significant.

Study approval. All procedures involving animals were performed in accordance with the guidelines of the IACUC of KU Leuven and approved in project application (PO34/2014).

Author contributions

MO, JCT, and FL acquired and analyzed the data. MO and BB performed most of the genomics analysis. MO, JCT, and SL performed the in vitro/in cellulo experiments. FL and MO performed the in vivo experiments. JW and JJVDO optimized and performed FES IHC and analyzed the TMA data. FR performed biostatistical analysis and provided the microarray data. S Aibar analyzed the RNA-sequencing data. BT performed the bioinformatic analysis of hypermethylation. JB contributed to some of the Western blot analyses. CK performed epidermal whole-mount immunostaining. ER performed IHC analysis of mouse tissues. S Aerts contributed to the design of some of the bioinformatics analyses and edited the manuscript. PDS, PD, and STD contributed to the design of some of the experiments and edited the manuscript. DL designed the genomics study and some of the bioinformatics analyses and supervised the mouse sequencing experiments. JCM designed most of the experiments and wrote the manuscript.

Acknowledgments

We thank G. Bervoets, O. Van Goethem, S. Peeters, J. Agopian, D. Smeets, G. Peuteman, and T. Van Brussel for excellent technical assistance. We thank M. Dewaele for his contribution and technical assistance. We thank R. Marais and L. Sommer for providing some of the mouse melanoma samples. RNA sequencing was performed by the VIB Nucleomics Core facility (www.nucleomics.be). This work was supported in part by FWO (grant G.0689.12N to JCM; grant G.0791.14 to S. Aerts); the Interuniversitaire Attractiepolen (IUAP); the Special Research Fund (BOF) KU Leuven (grant PF/10/016 to S. Aerts); the Foundation Against Cancer (grant 2014-126 to JCM; grant 2012-F2 to S. Aibar); the Fondation ARC (grant PJA2013120021 to PDS); La Ligue Contre le Cancer (Equipe Labélisée to PD and PDS). FL and CK are recipients of Fund for Scientific Research Flanders (FWO) postdoctoral and PhD fellowships, respectively. MO and JB are recipients of PhD fellowships from the VIB PhD international program. FR is a recipient of a postdoctoral fellowship from the Marie-Curie/VIB OMICs program. JCT was supported by PhD fellowships from the French Ministry of Research and the Fondation pour la Recherche Médicale(FDT20150532362). JW received funding from the Melanoma Research Alliance (Team Science Research Award; USA) and is currently funded as an Emmanuel van der Schueren postdoctoral researcher by Kom op tegen Kanker.

Address correspondence to: Diether Lambrechts, O&N IV Herestraat 49/Box 912, 3000 Leuven, Belgium. Phone: 32.16.37.32.09; E-mail: diether.lambrechts@kuleuven.vib.be. Or to: Paulo De Sepulveda, CRCM – Inserm, 27 Bd Leï Roure, 13009 Marseille, France. Phone: 33.4.86977285; E-mail: sepulveda@inserm.fr. Or to: Jean-Christophe Marine, O&N IV Herestraat 49/Box 602, 3000 Leuven, Belgium. Phone: 32.16.33.03.68; Phone: jeanchristophe.marine@kuleuven.vib.be.

1. Lawrence MS, et al. Mutational heterogeneity in cancer and the search for new cancer-associated genes. *Nature*. 2013;499(7457):214–218.
2. Hanahan D, Weinberg RA. Hallmarks of cancer: the next generation. *Cell*. 2011;144(5):646–674.
3. Grob JJ, Long GV, Schadendorf D, Flaherty K. Disease kinetics for decision-making in advanced melanoma: a call for scenario-driven strategy trials. *Lancet Oncol*. 2015;16(13):e522–e526.
4. Hodis E, et al. A landscape of driver mutations in melanoma. *Cell*. 2012;150(2):251–263.
5. Davies H, et al. Mutations of the BRAF gene in human cancer. *Nature*. 2002;417(6892):949–954.
6. Hocker T, Tsao H. Ultraviolet radiation and melanoma: a systematic review and analysis of reported sequence variants. *Hum Mutat*. 2007;28(6):578–588.
7. Jakob JA, et al. NRAS mutation status is an independent prognostic factor in metastatic melanoma. *Cancer*. 2012;118(16):4014–4023.
8. Krauthammer M, et al. Exome sequencing identifies recurrent somatic RAC1 mutations in melanoma. *Nat Genet*. 2012;44(9):1006–1014.
9. Dhomen N, et al. Oncogenic Braf induces melanocyte senescence and melanoma in mice. *Cancer Cell*. 2009;15(4):294–303.
10. Cohen C, et al. Mitogen-actived protein kinase activation is an early event in melanoma progression. *Clin Cancer Res*. 2002;8(12):3728–3733.
11. Flaherty KT, Hodi FS, Bastian BC. Mutation-driven drug development in melanoma. *Curr Opin Oncol*. 2010;22(3):178–183.
12. Chapman PB, et al. Improved survival with vemurafenib in melanoma with BRAF V600E mutation. *N Engl J Med*. 2011;364(26):2507–2516.
13. Ackermann J, Frutschi M, Kaloulis K, McKee T, Trumpp A, Beermann F. Metastasizing melanoma formation caused by expression of activated N-RasQ61K on an INK4a-deficient background. *Cancer Res*. 2005;65(10):4005–4011.
14. Dankort D, et al. Braf(V600E) cooperates with Pten loss to induce metastatic melanoma. *Nat Genet*. 2009;41(5):544–552.
15. Shakhova O, et al. Sox10 promotes the formation and maintenance of giant congenital naevi and melanoma. *Nat Cell Biol*. 2012;14(8):882–890.
16. Cancer Genome Atlas Network. Genomic Classification of Cutaneous Melanoma. *Cell*. 2015;161(7):1681–1696.
17. Damsky WE, et al. β-catenin signaling controls metastasis in Braf-activated Pten-deficient melanomas. *Cancer Cell*. 2011;20(6):741–754.
18. Gembarska A, et al. MDM4 is a key therapeutic target in cutaneous melanoma. *Nat Med*. 2012;18(8):1239–1247.
19. Viros A, et al. Ultraviolet radiation accelerates BRAF-driven melanomagenesis by targeting TP53. *Nature*. 2014;511(7510):478–482.
20. Conde-Perez A, et al. A caveolin-dependent and PI3K/AKT-independent role of PTEN in β-catenin transcriptional activity. *Nat Commun*. 2015;6:8093.
21. Krimpenfort P, Quon KC, Mooi WJ, Loonstra A, Berns A. Loss of p16Ink4a confers susceptibility to metastatic melanoma in mice. *Nature*. 2001;413(6851):83–86.
22. Jacks T, et al. Tumor spectrum analysis in p53-mutant mice. *Curr Biol*. 1994;4(1):1–7.
23. Nassar D, Latil M, Boeckx B, Lambrechts D, Blanpain C. Genomic landscape of carcinogen-induced and genetically induced mouse skin squamous cell carcinoma. *Nat Med*. 2015;21(8):946–954.
24. Olive KP, et al. Mutant p53 gain of function in two mouse models of Li-Fraumeni syndrome. *Cell*. 2004;119(6):847–860.
25. Briscoe J, Thérond PP. The mechanisms of Hedgehog signalling and its roles in development and disease. *Nat Rev Mol Cell Biol*. 2013;14(7):416–429.
26. Ma C, et al. Characterization CSMD1 in a large set of primary lung, head and neck, breast and skin cancer tissues. *Cancer Biol Ther*. 2009;8(10):907–916.
27. McFadden DG, et al. Genetic and clonal dissection of murine small cell lung carcinoma progression by genome sequencing. *Cell*. 2014;156(6):1298–1311.
28. Zemach A, McDaniel IE, Silva P, Zilberman D. Genome-wide evolutionary analysis of eukaryotic DNA methylation. *Science*. 2010;328(5980):916–919.
29. Feng S, et al. Conservation and divergence of methylation patterning in plants and animals. *Proc Natl Acad Sci USA*. 2010;107(19):8689–8694.
30. Vogelstein B, Papadopoulos N, Velculescu VE, Zhou S, Diaz LA, Kinzler KW. Cancer genome landscapes. *Science*. 2013;339(6127):1546–1558.
31. McNeal AS, et al. CDKN2B Loss Promotes Progression from Benign Melanocytic Nevus to Melanoma. *Cancer Discov*. 2015;5(10):1072–1085.
32. Maertens O, et al. Elucidating distinct roles for NF1 in melanomagenesis. *Cancer Discov*. 2013;3(3):338–349.
33. Liu W, et al. LKB1/STK11 inactivation leads to expansion of a prometastatic tumor subpopulation in melanoma. *Cancer Cell*. 2012;21(6):751–764.
34. Viros A, et al. Ultraviolet radiation accelerates BRAF-driven melanomagenesis by targeting TP53. *Nature*. 2014;511(7510):478–482.
35. Cao J, et al. The E3 ligase APC/C(Cdh1) promotes ubiquitylation-mediated proteolysis of PAX3 to suppress melanocyte proliferation and melanoma growth. *Sci Signal*. 2015;8(392):ra87.
36. Jiao J, Fan Y, Zhang Y. Expression and clinicopathological significance of microRNA-21 and programmed cell death 4 in malignant melanoma. *J Int Med Res*. 2015;43(5):672–678.
37. Cheng PF, Dummer R, Levesque MP. Data mining The Cancer Genome Atlas in the era of precision cancer medicine. *Swiss Med Wkly*. 2015;145:w14183.
38. Rambow F, et al. New functional signatures for understanding melanoma biology from tumor cell lineage-specific analysis. *Cell Rep*. 2015;13(4):840–853.
39. Bendl J, Musil M, Štourač J, Zendulka J, Damborský J, Brezovský J. PredictSNP2: a unified platform for accurately evaluating snp effects by exploiting the different characteristics of variants in distinct genomic regions. *PLoS Comput Biol*. 2016;12(5):e1004962.
40. Winnepenninckx V, et al. Gene expression profiling of primary cutaneous melanoma and clinical outcome. *J Natl Cancer Inst*. 2006;98(7):472–482.
41. Delfino FJ, Stevenson H, Smithgall TE. A growth-suppressive function for the c-fes protein-tyrosine kinase in colorectal cancer. *J Biol Chem*. 2006;281(13):8829–8835.
42. Zirngibl RA, Senis Y, Greer PA. Enhanced endotoxin sensitivity in fps/fes-null mice with minimal defects in hematopoietic homeostasis. *Mol Cell Biol*. 2002;22(8):2472–2486.
43. Spranger S, Bao R, Gajewski TF. Melanoma-intrinsic β-catenin signalling prevents anti-tumour immunity. *Nature*. 2015;523(7559):231–235.
44. Widlund HR, et al. Beta-catenin-induced melanoma growth requires the downstream target Microphthalmia-associated transcription factor. *J Cell Biol*. 2002;158(6):1079–1087.
45. Cheli Y, Ohanna M, Ballotti R, Bertolotto C. Fifteen-year quest for microphthalmia-associated transcription factor target genes. *Pigment Cell Melanoma Res*. 2010;23(1):27–40.
46. Dudgeon C, et al. The evolution of thymic lymphomas in p53 knockout mice. *Genes Dev*. 2014;28(23):2613–2620.
47. Lee WH, Bister K, Pawson A, Robins T, Moscovici C, Duesberg PH. Fujinami sarcoma virus: an avian RNA tumor virus with a unique transforming gene. *Proc Natl Acad Sci USA*. 1980;77(4):2018–2022.
48. Voisset E, Lopez S, Dubreuil P, De Sepulveda P. The tyrosine kinase FES is an essential effector of KITD816V proliferation signal. *Blood*. 2007;110(7):2593–2599.
49. Craig AW. FES/FER kinase signaling in hematopoietic cells and leukemias. *Front Biosci (Landmark Ed)*. 2012;17:861–875.
50. Bardelli A, et al. Mutational analysis of the tyrosine kinome in colorectal cancers. *Science*. 2003;300(5621):949.
51. Sangrar W, Zirgnibl RA, Gao Y, Muller WJ, Jia Z, Greer PA. An identity crisis for fps/fes: oncogene or tumor suppressor? *Cancer Res*. 2005;65(9):3518–3522.
52. Easty DJ, Herlyn M, Bennett DC. Abnormal protein tyrosine kinase gene expression during melanoma progression and metastasis. *Int J Cancer*. 1995;60(1):129–136.
53. Fleuren ED, Zhang L, Wu J, Daly RJ. The kinome 'at large' in cancer. *Nat Rev Cancer*. 2016;16(2):83–98.
54. Davis MI, et al. Comprehensive analysis of kinase inhibitor selectivity. *Nat Biotechnol*. 2011;29(11):1046–1051.

55. Hellwig S, et al. Small-molecule inhibitors of the c-Fes protein-tyrosine kinase. *Chem Biol*. 2012;19(4):529–540.
56. Anastassiadis T, Deacon SW, Devarajan K, Ma H, Peterson JR. Comprehensive assay of kinase catalytic activity reveals features of kinase inhibitor selectivity. *Nat Biotechnol*. 2011;29(11):1039–1045.
57. Rimm DL, Caca K, Hu G, Harrison FB, Fearon ER. Frequent nuclear/cytoplasmic localization of beta-catenin without exon 3 mutations in malignant melanoma. *Am J Pathol*. 1999;154(2):325–329.
58. Omholt K, Platz A, Ringborg U, Hansson J. Cytoplasmic and nuclear accumulation of beta-catenin is rarely caused by CTNNB1 exon 3 mutations in cutaneous malignant melanoma. *Int J Cancer*. 2001;92(6):839–842.
59. Forbes SA, et al. COSMIC (the Catalogue of Somatic Mutations in Cancer): a resource to investigate acquired mutations in human cancer. *Nucleic Acids Res*. 2010;38(Database issue):D652–D657.
60. Larue L, Delmas V. The WNT/Beta-catenin pathway in melanoma. *Front Biosci*. 2006;11:733–742.
61. Delmas V, et al. Beta-catenin induces immortalization of melanocytes by suppressing p16INK4a expression and cooperates with N-Ras in melanoma development. *Genes Dev*. 2007;21(22):2923–2935.
62. Pandolfi S, Montagnani V, Lapucci A, Stecca B. HEDGEHOG/GLI-E2F1 axis modulates iASPP expression and function and regulates melanoma cell growth. *Cell Death Differ*. 2015;22(12):2006–2019.
63. Jalili A, et al. NVP-LDE225, a potent and selective SMOOTHENED antagonist reduces melanoma growth in vitro and in vivo. *PLoS One*. 2013;8(7):e69064.
64. Stecca B, et al. Melanomas require HEDGEHOG-GLI signaling regulated by interactions between GLI1 and the RAS-MEK/AKT pathways. *Proc Natl Acad Sci U S A*. 2007;104(14):5895–5900.
65. Bosenberg M, et al. Characterization of melanocyte-specific inducible Cre recombinase transgenic mice. *Genesis*. 2006;44(5):262–267.
66. Dankort D, Filenova E, Collado M, Serrano M, Jones K, McMahon M. A new mouse model to explore the initiation, progression, and therapy of BRAFV600E-induced lung tumors. *Genes Dev*. 2007;21(4):379–384.
67. Mercer K, et al. Expression of endogenous oncogenic V600EB-raf induces proliferation and developmental defects in mice and transformation of primary fibroblasts. *Cancer Res*. 2005;65(24):11493–11500.
68. Lesche R, et al. Cre/loxP-mediated inactivation of the murine Pten tumor suppressor gene. *Genesis*. 2002;32(2):148–149.
69. Jonkers J, Meuwissen R, van der Gulden H, Peterse H, van der Valk M, Berns A. Synergistic tumor suppressor activity of BRCA2 and p53 in a conditional mouse model for breast cancer. *Nat Genet*. 2001;29(4):418–425.
70. Srinivas S, et al. Cre reporter strains produced by targeted insertion of EYFP and ECFP into the ROSA26 locus. *BMC Dev Biol*. 2001;1:4.
71. Serrano M, Lee H, Chin L, Cordon-Cardo C, Beach D, DePinho RA. Role of the INK4a locus in tumor suppression and cell mortality. *Cell*. 1996;85(1):27–37.
72. Fenouille N, et al. The epithelial-mesenchymal transition (EMT) regulatory factor SLUG (SNAI2) is a downstream target of SPARC and AKT in promoting melanoma cell invasion. *PLoS One*. 2012;7(7):e40378.
73. Tichet M, et al. Tumour-derived SPARC drives vascular permeability and extravasation through endothelial VCAM1 signalling to promote metastasis. *Nat Commun*. 2015;6:6993.
74. Mascré G, et al. Distinct contribution of stem and progenitor cells to epidermal maintenance. *Nature*. 2012;489(7415):257–262.
75. Li H, Durbin R. Fast and accurate short read alignment with Burrows-Wheeler transform. *Bioinformatics*. 2009;25(14):1754–1760.
76. McKenna A, et al. The Genome Analysis Toolkit: a MapReduce framework for analyzing next-generation DNA sequencing data. *Genome Res*. 2010;20(9):1297–1303.
77. Albertson DG, Collins C, McCormick F, Gray JW. Chromosome aberrations in solid tumors. *Nat Genet*. 2003;34(4):369–376.
78. Wang K, Li M, Hakonarson H. ANNOVAR: functional annotation of genetic variants from high-throughput sequencing data. *Nucleic Acids Res*. 2010;38(16):e164.
79. Wang K, et al. PennCNV: an integrated hidden Markov model designed for high-resolution copy number variation detection in whole-genome SNP genotyping data. *Genome Res*. 2007;17(11):1665–1674.
80. Van Loo P, et al. Allele-specific copy number analysis of tumors. *Proc Natl Acad Sci U S A*. 2010;107(39):16910–16915.
81. Mermel CH, Schumacher SE, Hill B, Meyerson ML, Beroukhim R, Getz G. GISTIC2.0 facilitates sensitive and confident localization of the targets of focal somatic copy-number alteration in human cancers. *Genome Biol*. 2011;12(4):R41.